International Journal of Engineering and Advanced Technology (IJEAT)
ISSN: 2249-8958 (Online), Volume-8 Issue-5, June 2019

Development of polymer matrix decorated In_2O_3 particles it's electrical and optical

Naser hussein judran, Ajeet Kumar

Abstract ***Indium tin oxide (ITO) nanoparticles were synthesized by co-precipitation method using ammonium hydroxide as precipitator. The synthesized nanoparticles were investigated by scanning electron microscopy, activation of energy measurement and X-ray diffractometry (XRD) techniques. THE XRD patterns of nanoparticles were also studied by scherrer formula for calculation of crystallite size. Nanoparticles with the excitation energy lower than their band gaps. It was found that the ratios of temperature bands have relation with conductivity of ITO nanoparticles. The band gap in structure of ITO nanoparticles was described considering the obtained results.***

Key words:- Sn – doped In_2O_3 that would be used as an electrical conductor.

I. NTRODUCTION

1.1 Indium oxide (In_2O_3)

1.1.1 An Introduction to the oxide material

Indium oxide (In_2O_3) is a technologically important transparent conducting oxide (TCO) material. Indium oxide is an n-type semiconductor with wide energy band gap in the range of 3.60-3.72. The structure of In_2O_3 in its crystalline form is body centered cubic (bcc) with a lattice constant of about 10.11 Å [1]. The increasing interest in the interaction of light with electricity and electronically active materials made the materials and techniques for producing semitransparent electrically conducting films particularly attractive. Transparent conductors have found major applications in a number of electronic and optoelectronic devices including resistors, transparent heating elements, antistatic and electromagnetic shield coatings, transparent electrode for solar cells, antireflection coatings, heat reflecting mirrors in glass windows and many others [2-11]. Tin doped indium oxide (indium tin oxide or ITO) is one of the most commonly used transparent conducting oxides. At present and likely well into the future this material offers best available performance in terms of conductivity and transmittivity combined with excellent environmental stability, reproducibility and good surface morphology. High optical transparency in the visible region more than 80%, low electrical resistivity less than 10^{-3} Ωcm and high infrared reflectivity make indium oxide (In_2O_3) a choice for many potential applications in the upcoming nanoelectronic building blocks.

Manuscript published on 30 June 2019.
***** Correspondence Author (s)
Naser hussein judran, Department of Physics, SHIATS, Allahabad. (Uttar Pradesh), India.
Mr. Ajeet Kumar, Department of Physics, SHIATS, Allahabad. (Uttar Pradesh), India.

In_2O_3 is an n-type semiconductor with a wide band gap of about 3.6 eV that exhibits many size- and shape-dependent properties, based on which many new applications have been also explored. Indium oxide has C-type rare earth oxide structure those crystallites in the ordered vacancy structure with eight formula units. Among the 16 In atoms 1/4 of the In atoms (In1) occupy the centers of the trigonally distorted octahedra (Wyckoff 8b position) and 3/4 of In atoms (In2) occupy the centers of tetragonally distorted octahedra (Wyckoff 24d position) that ensure a good packing ratio [12]. In addition, In_2O_3 has single free electron-like band of s-character forming the bottom of the conduction band hybridized with highly dispersed O 2s states. The valence band edge arises from the O 2p states hybridized with In2 5d. This intriguing band structure results in uniform distribution of the charge that reduces the scattering to a minimum. Moreover, the high electrical conductivity due to mobility enhancement and Burstein–Moss shift can also be explained on the basis of dispersion of these bands. These interesting optical and electrical properties tailored to occur due to the modified structural packing and band structure makes this material suitable for many novel optoelectronic device fabrications.

1.1.2 Optical properties of In_2O_3

Although partial transparency, with a reduction in conductivity, can be obtained for very thin metallic films, high transparency and simultaneously high conductivity cannot be attained in intrinsic stoichiometric materials. The only way this can be achieved is by creating electron degeneracy in a wide band gap (Eg > 3eV or more for visible radiation) material by controllably introducing non-stoichiometry and/or appropriate dopants [13-18]. These conditions can be conveniently met for In_2O_3 as well as a number of other materials like Zinc oxide, Cadmium oxide etc. In_2O_3 shows interesting and technologically important combination of properties viz. high luminous transmittance, high IR reflectance, good electrical conductivity, excellent substrate adherence and chemical inertness. In_2O_3 is a key part of solar cells, window coatings, energy efficient buildings, and flat panel displays. In solar cells, In_2O_3 can be the transparent, conducting top layer that lets light into the cell to shine the junction and lets electricity flow out. Improving the In_2O_3 layer can help improve the solar cell efficiency. A transparent conducting oxide is a material with high transparency in a derived part of the spectrum and high electrical conductivity. Beyond these key properties of transparent conducting oxides (TCOs), In_2O_3 has a number of other key characteristics. The structure of In_2O_3 can be amorphous, crystalline, or mixed, depending on the deposition temperature and atmosphere. The electro-optical properties are a function of the crystallinity of the material. In general,

In_2O_3 deposited at room temperature is amorphous, and In_2O_3 deposited at higher temperatures is crystalline. Depositing at high temperatures is more expensive than at room temperature, and this method may not be compatible with the underlying devices.

Among other effects, doping TCO films can induce a shift in the band gap. In heavily doped n-type semiconductors, the shift is due to the competitive effects of the Burstein–Moss (BM) band filling and the fundamental band gap narrowing (BGN). Narrowing of the fundamental gap is the result of many-body effects and is also known as band gap renormalization. Good agreement between theory and experiment for the band gap shift of heavily doped group IV, III-V, and II-VI semiconductors have been demonstrated [19-27]. For pure In_2O_3 films, the band gap shift has been extensively studied using the Burstein–Moss (BM) theory while accounting for the many-body effects. However, for heavily doped In_2O_3, there has not yet been a systematic report on the dopant-induced band gap shift which also accounts for the nonparabolicity of the conduction band. Various investigations seem to leave out the nonparabolicity or ignore the band gap renormalization. For a complete understanding of the band gap shift in doped In_2O_3, an effective theoretical model is needed which considers BGN and a non parabolic BM shift simultaneously.

1.2 Research background on indium oxide as a semiconductor material

1.2.1 In_2O_3 as a material in semiconductor industry

Rapid and significant advances have been taking place in the field of semiconductor physics during the past few decades. In the field of research and industry, semiconductors are the subject of great interest because of their numerous practical applications. Scientists are interested in developing those materials, which maintain their required properties under extreme environmental conditions [28-35]. One of the most important fields of current interest in material science is the fundamental aspects and applications of semiconducting transparent thin films. Such materials are highly conducting and exhibit high transparency in the visible region of the electromagnetic spectrum. Because of this unique property, transparent conducting oxides (TCOs) are finding wide range of applications in research and industry. They are essential part of technologies that require large area electrical contact and optical access in the visible portion of the light spectrum. A TCO is a wide band gap semiconductor that has relatively high concentration of free electrons in the conduction band. These arise either from defects in the material or from extrinsic dopants, the impurity levels of which lie near the conduction band edge. The high carrier concentration [36] causes absorption of electromagnetic radiations in both visible and IR portions of the spectrum. A TCO must necessarily represent a compromise between electrical conductivity and optical transmittance; a careful balance between these properties is required. Reduction of the resistivity involves either an increase in carrier concentration or in the mobility. But increase in the former will lead to an increase in the visible absorption while the increase in mobility has no adverse effect on the optical properties. So the search for new TCO materials must focus on achieving materials with higher electron motilities. The above target can be achieved by making material with longer electron relaxation times or by identifying materials with lower electron effective masses.

Most of the useful oxide-based materials are n-type conductors that ideally have a wide band gap (>3 eV), the ability to be doped to degeneracy, and a conduction band shape that ensures that the plasma absorption edge lies in the infrared range [37]. The transparency of the TCO films in the visible region is a result of the wide band gap of the material and the n type conductivity is mainly due to the oxygen ion vacancies that contribute to the excess electrons in the metal. Numerous investigations have been made on the electrical properties of transparent conducting oxide films to understand the conduction phenomena involved [38-45]. Researchers have made a systematic study on the effect of various parameters such as nature and temperature of the substrate, film thickness, dopant and its concentration etc [46-49] on the electrical properties of TCO films in order to optimize the growth conditions. The high conductivity of the TCO films results mainly from stoichiometric deviation. The conduction electrons in these films are supplied from donor sites associated with oxygen vacancies or excess metal ions [50]. These donor sites can be easily created by chemical reduction. Unintentional doping which happens mainly in the case of film deposition by spray pyrolysis, intentional doping and contamination by alkali ions from the glass substrate can affect electrical conductivity. One of the major factors governing the conductivity of TCO films is the carrier mobility. The mobility of the carriers in the polycrystalline film is dependent on the mechanism by which carriers are scattered by lattice imperfections. The various scattering mechanisms involved in semiconducting thin films are acoustic deformation potential scattering, piezoelectric scattering, optical phonon scattering, neutral impurity scattering, ionized impurity scattering, electron-electron scattering and grain boundary scattering [51-57]. In the case of a polycrystalline film, the conduction mechanism is dominated by the inherent inter-crystalline boundaries rather than the intra-crystalline characteristics. These boundaries generally contain fairly high densities of interface states which trap free carriers by virtue of the inherent disorders and the presence of trapped charges. The interface states results in a space charge region in the grain boundaries. Due to this space charge region, band bending occurs, resulting in potential barriers to charge transport.

1. 2. 2 Transparent Conducting Oxide (TCO) materials

Transparent conducting oxides (TCOs) are electrical conductive materials with a comparably low absorption of light. They are usually prepared with thin film technologies and used in opto-electrical devices such as solar cells, displays, opto-electrical interfaces and circuitries. Glass fibers are nearly lossless conductors of light, but electrical insulators; silicon and compound semiconductors are wavelength dependent optical resistors (generating mobile electrons), but dopant dependent electrical conductors [58-59]. Transparent conducting oxides are highly flexible intermediate states with both these characteristics. Their conductivity can be tuned from insulating via semiconducting to conducting as well as their transparency adjusted. As they can be produced as n-type and p-type conductive, they open a wide range of power saving opto-electrical circuitries and technological applications.

TCOs on window glass improve the energy efficiency of the window because free electrons reflect infrared radiation for wavelengths longer than the plasma wavelength. In cold climates, the plasma wavelength of about 2μm is desirable, so that most of the solar spectrum is transmitted to heat inside the building. Fluorine-doped tin oxide is the best material for this since it combines a suitable plasma wavelength with excellent durability and low cost. In hot climates, the plasma wavelength, about 1 μm is desirable, so that the near-infrared portion of incident sunlight can be reflected out of the building [60-64]. Silver and titanium nitride is widely used for this application. Transparent conducting oxide (TCO) materials have been widely used in different areas due to their high optical transparency, low resistivity and wide energy band gap and hence there has been great deal of work on investigating their preparation processes and optimizing their properties. Various ternary and compound oxide materials have been developed and obtained good opto-electronic transport properties. But the preparation of doped ternary and multi-component oxide layers with suitable composition and understanding of the chemistry involved are rather difficult when compared to undoped TCO materials. In general, undoped binary oxide films are insulators in its stoichiometric condition [65]. But the conductivity of pure oxide layers can be improved to the level of doped layers by suitably controlling the density of oxygen vacancies, each of which donate two electrons to the conduction band. This deficiency determines the conductivity of undoped oxide layers. Moreover, the ultimate attainable properties are material dependent. Among the various TCO materials available, In_2O_3 is one of the potential candidates for solar cell and sensor applications. It is an n-type semiconductor that has high electrical conductivity. This material has an optical energy band gap of 3.6 eV with good adherence to the substrate surface and high chemical inertness.

1.3 Applications of In_2O_3

1.3.1 Solar cell fabrication industry

The front surfaces of solar cells are covered by transparent electrodes. Thermal stability and low cost are the primary factors in this choice. The high work function of SnO_2: F is also helpful in making low-resistance electrical contact to the p-type amorphous-silicon layer. Amorphous-silicon cells are grown on flexible steel or plastic substrates; in this case, the top TCO must be deposited at low temperature on thermally sensitive cells. ITO or ZnO is chosen for this purpose because both compounds can be deposited successfully at low temperatures. Etchability is a very important consideration in forming patterns in the TCO electrode. The easier etchability of ITO has favored its use over tin oxide which is more difficult to etch. The low deposition temperature of ITO is also a factor for color displays in which the TCO is deposited over thermally sensitive organic dyes. Low resistance is another factor favoring ITO in very finely patterned displays, since the ITO layer can be made very thin, thus the etched topography remains fairly smooth. Freezers in supermarkets pass electric current through TCOs on their display windows in order to prevent moisture in the air from condensing on them and obscuring the view. Low cost and durability are the main factors that make tin oxide a favourable choice for the application. ITO is used in modern cockpits because its lower resistance permits defrosting larger window areas with relatively low voltage (24 V). Some automobile windshields use silver or silver copper alloy TCOs for electrical defrosting because the systems in automobiles require very low resistance, combined with the legal requirement of a minimum transmission of 70%. Tin oxide coatings are placed on oven windows to improve their safety by lowering the outside temperature of the glass to safe levels [66-69]. The tin oxide coating also improves the energy efficiency of the ovens. The main criteria for this choice of material are high temperature stability, chemical and mechanical durability, and low cost.

1.3.2 Indium oxide as a suitable material for various gas sensor applications Metal oxide semiconductor gas sensors are the most promising devices among the solid state chemical sensors because of their small dimensions, low power consumption, high sensor response, low detection limit, and high compatibility with microelectronic processing. The gas sensing mechanism of oxide sensors is mainly attributed to the oxidation/reduction redox properties which are controlled by the surface. In case of bulk and thin film oxides, changes in grain size, porosity, thickness, voids, and stoichiometry affect the gas sensing properties. In case of nanostructures, it is possible to control the crystallinity and stoichiometry during the growth process which allows for the manipulation of these crucial parameters that control the gas sensing properties [70-74]. The morphology and size of the oxide nanostructures has also been reported to play an important role in determining the gas sensing properties. Any change in surface chemistry may directly affect the gas sensing properties of one-dimensional (1D) nanostructures. Indium oxide has been suggested as a highly sensitive gas sensor toward target gases and is selected as prototype metal oxide for gas sensing applications. Gas sensors based on Indium oxide thin films have been reported in the literature. Jun Tamaki et al. [75] have report the chlorine sensing properties of In_2O_3 thin films prepared by electron beam evaporation technique. Wan-Young Chung et al. [76] have grown Indium oxide thin films on silicon and Alumina substrates and have discussed its CO, H_2 and C_3H_8 sensing properties. Low temperature indium oxide sensors have been fabricated by R. Winter et al. through molecular beam epitaxy technique and the films show significant response for a number of gases including NH_3 and NO_2 [77]. Indium oxide films have also been tested for ozone gas by M.Suchea et al. [78].

1.3.3 In_2O_3 as a material for organic light emitting diode (OLED) applications

Various kinds of transparent conducting oxide (TCO) thin films such as zinc oxide, impurity-doped indium oxides and tin oxides have been widely used as transparent conductors for many opto-electronic applications [79]. Indium oxide provides good electrical conductivity and high transparency in the visible region hence it is the most commonly used electrode material in flat panel displays. Moreover for organic electronics such as organic light-emitting diodes (OLEDs), organic solar cells and organic thin film transistors, In_2O_3 is the best suited anode material as it provides good energy-level matching for the efficient injection of holes into the organic layers [80]. These OLEDs have more brightness, high efficiency, a wide viewing angle, and quick response time. Currently, organic devices are fabricated on rigid substrates and then encapsulated with glass lid.

Published By:
Blue Eyes Intelligence Engineering
& Sciences Publication (BEIESP)

Alternatively, fabricating the devices on plastic substrates increases the number of OLED applications. Transparent conducting indium oxide thin films on flexible substrates have many applications. They can be used in plastic liquid crystal display devices, transparent electro-magnetic shielding materials, flexible electro-optical devices, heat reacting mirrors, etc. These flexible substrates may be paper, thin aluminum foil or polymer (PET, PEN, MYLAR, Transphan and polycarbonate.

Due to the poor thermal endurance of plastic substrates, In_2O_3 films are deposited at low temperature. Also, low temperature deposition improves the electrical as well as optical properties of In_2O_3, increases the efficiency of devices. A few researchers have reported In_2O_3 film deposited at low substrate temperature by different techniques, especially by sputtering [81]. Fan reported a resistivity as low as 5.5 $x10^{-4}$ Ω cm and the transmittance over 80% for films deposited at substrate temperature below 1000°C by ion-beam sputtering [82]. Mansingh and Vasant Kumar reported a resistivity of $1x10^{-3}$ Ω cm for films deposited on water-cooled Mylar by RF sputtering [83].

1.4 Opto-electronic applications

1.4.1 Photovoltaic applications of indium oxide

Dye-sensitized solar cells (DSSCs) have attracted much attention as promising alternatives to conventional solar energy conversion devices because of their low cost of production and high energy conversion efficiency. Transparent conductive oxide (TCO) layers, which collect charge carriers from TiO_2 and transfer them to the external electric circuit, are one of the most important components of a solar cell because low charge collecting efficiency of a TCO layer may deteriorate the cell performance [84-89]. Therefore, TCO layers have been studied extensively to understand the nature of the TiO_2/TCO interface and to improve the charge collecting efficiency.

Because of good electrical conductivity at room temperature and high transparency in the visible range, indium oxide films have been extensively used as transparent electrodes in electronics and optoelectronics applications, including heaters in windows, sensors, flat panel displays, and solar cells. However, In_2O_3 films are unfavorable for use in DSSCs because the charge collection properties of films are significantly destroyed after an annealing process in conventional air; photo electrodes that consist of a TiO_2 film and a TCO layer should be annealed in an oxidizing atmosphere with a temperature over 300 °C to interconnect the TiO_2 nanoparticles, adhere the TiO_2 film to the TCO layer, and remove residual organics from the TiO_2 nanoparticle layer.

The electrical conductivity originates from free carriers that are generated by the following lattice defects:

(i) Sn^{4+} ion in an In^{3+} site, and

(ii) Vacancies in the regular oxygen lattice.

Justification: The deterioration in conductivity of In_2O_3 during annealing has been attributed to oxygen from the atmosphere filling a portion of the oxygen vacancies in the film. Therefore, there have been significant efforts to block the penetration of oxygen into these films, for example, by forming a fluorine-doped tin oxide (FTO)/ITO double layer, a SnO_2/ITO double layer, and a TiO_2/ antimony-doped tin oxide (ATO)/ITO triple layer.

A simple way to conserve the electrical conductivity of indium oxide films is to anneal them in a reducing H_2 atmosphere, thereby preventing annihilation of oxygen vacancies. In the present study, deteriorated TiO_2/ITO electrode (by oxidation annealing process) was annealed in an H_2 atmosphere in order to generate the oxygen vacancy again, that is, to recover the conductivity of the film. However, the TiO_2 film could be also reduced by the H_2 annealing which could decrease the performance of the DSSC by generating defects in the film. The electrochemical oxidation method to remove defects while conserving the electrical conductivity of In_2O_3 has been investigated by many researchers so far [90].

1.4.2 Properties of In_2O_3 using polymer as a substrate material

Recently, there has been increasing interest in depositing In_2O_3 on polymer substrates for light-emitting diode (LED) , organic light-emitting devices (OLED), and liquid crystal display (LCD) applications. Compared with the traditional glass substrate, polymer substrates provide displays that are lighter in weight and more resistant to impact damage, making them suitable for portable devices. An LCD or OLED built on flexible materials, such as metal and plastic, can be made into any shape, making it ideal for a car dashboard or a handy roll-up. Though the technical hurdles are significant, flexible displays could lead to major gains in manufacturing efficiency. Instead of relying on batch processes used for LCDs, the displays could be made on roll-to-roll continuous-processing equipment, much like the printers are used to print newspapers.

1.4.3 Use of In_2O_3 as an electro chromic material

Electrochromism, a reversible change in a material's optical properties (transmittance, absorbance and reflectance) under an applied voltage [91], is a phenomenon which was discovered many years ago. Since its discovery, considerable progress has been achieved in the syntheses of electrochromic (EC) materials, the fabrications of EC devices, the improvements of EC properties and the applications of EC materials that have been extended to smart windows, displays, antiglare mirrors and active camouflages [92]. Among them, smart windows represent an important application because they can effectively save energy by regulating solar heat gain, and provide indoor comfort by reversible color changes. EC smart windows have become more and more significant because the warming climate and energy crisis require a marked and substantial energy-saving to combat conventional energy source consumption.

Electrochromic devices are very interesting due to their possible application in architecture for an efficient use of energy in modern buildings where it is possible to control the flow of light and heat passing through the building glazing. ECDs can also be applied as glazing of vehicles, trains, and aircrafts and also as rearview mirrors already used in vehicles, as well as temperature control of frozen food.

EC devices have been discussed a long time, ever since the display-type devices presented shortly after the discovery of electrochromism in WO_3 films [93]. Generally speaking, the progress of technologies based on electrochromism has been slow, which may be associated with the necessity of simultaneously mastering a range of non-conventional technologies as follows:

The In_2O_3 material must combine excellent electrical conductivity with very low optical absorption, which is challenging especially for films on temperature sensitive substrates such as polymers.
(ii) The EC and counter electrode films must exhibit well specified nano porosities over large areas, which require non-standard coating technologies.
(iii) Viewing the EC device as a "thin film battery" makes is evident that charge insertion/extraction and charge balancing must be accomplished by properly controllable and industrially viable techniques,
such as gas treatments.
(iv) The electrolyte must combine good ion conductivity with adhesiveness and high transparency for ultraviolet irradiation.
(v) Long-term cycling durability demands adequate strategies for voltage and current control during coloration/bleaching—just as it does for charging/discharging of batteries.
All of these challenges can be successfully met, however, and EC technology finally may emerge as suitable for large-area, large-scale applications.

II. MATERIALS AND METHODS

3.1 INTRODUCTION

3.2 Variations in the oxygen partial pressure during the synthesis process of In_2O_3 samples affect not only the structure, but also the physical properties. Oxygen partial pressure has been found to be a key parameter in order to increase or decrease the density of oxygen vacancies. The oxygen vacancies act as donors, which leads to an increment in the carrier concentration. Variations in carrier concentration have a major impact on most of the physical properties of the materials [118]. Therefore, by altering the oxygen partial pressure during the growth process, it is possible to archive the desired structure, surface, interface, and many other physical properties of the nanostructures. Understanding the variations in the absorption and refractive index of an un-doped system with oxygen partial pressure is an essential step towards understanding the behaviour of the MCD and rotation of that system, and providing background knowledge for TM-doped systems. This chapter investigates the behaviour of oxygen impurity bands formed within the band gap energy of the host In_2O_3 in the absence of any effect originating from the TM 3d impurity band and related transitions. This will help us to predict and understand the impact of TM-doping and other growth conditions on In_2O_3 semiconductors. In addition, this chapter introduces a study about the tin-doping dependence of the optical and electrical properties of pure In_2O_3. Tin doping affects the In_2O_3 thin films because Sn^{4+} ions substitute In^{3+} ions and release an electron. Therefore, the carrier density increases with tin doping. Variations in the carrier concentration have a major impact on most of the physical properties. They can change the samples from an isolator to a metallic material through the semiconductor regime.

Indium oxide is an important transparent conducting oxide material (TCO). It is an insulator in its stoichiometric form, whereas in its non-stoichiometric form it behaves as a highly conducting semiconductor with a wide direct bandgap (E ≈3.6 eV).In recent decades, In_2O_3 has been widely applied in fabricating photovoltaic cells, sensor modules and transparent electrode materials for both electro-chromic cells and for liquid crystal display devices [119]. The current works for In_2O_3 are mainly concentrated on the preparation and studies of its doped films and powders [120-125]. Recently, significant interest has been focused on the field of preparing low-dimensional nanostructured semiconducting oxides for various applications. As well known, in semiconductors, the low-dimensional nanostructures such as quantum wires and quantum dots can improve drastically optoelectronic device performance [126].
Polymers have long been used as insulating materials. For example, metal cables are coated in plastic to insulate them. However, there are at least four major classes of semiconducting polymers that have been developed so far. They include conjugated conducting polymers, charge transfer polymers, ionically conducting polymers and conductively filled polymers. The conductively filled conducting polymers were first made in 1930 for the prevention of corona discharge. The potential uses for conductively filled polymers have since been multiplied due to their ease of processing, good environmental stability and wide range of electrical properties. Being a multi-phase system in nature, however, their lack of homogeneity and reproducibility has been an inherent weakness for conductively filled polymers. Therefore, controlling the quality of dispersion to obtain homogeneous conducting polymer composites is critically important.

3.3 CRYSTAL AND SURFACE STRUCTURE

Figure 3.1 shows the local structure of In_2O_3. It has a total of 80 atoms per unit cell, not all of which are depicted. The structure is body-centered cubic (Bixbyite) and has the space group Ia/3. The lattice constant is a = 10.117 Å. In the bixbyite structure, indium atoms occupy two symmetrically in equivalent sites denoted by their Wyckoff position. The In-b-site is at the body diagonal of the two oxygen vacancies in the upper right cube. For the In-b-site the coordination,

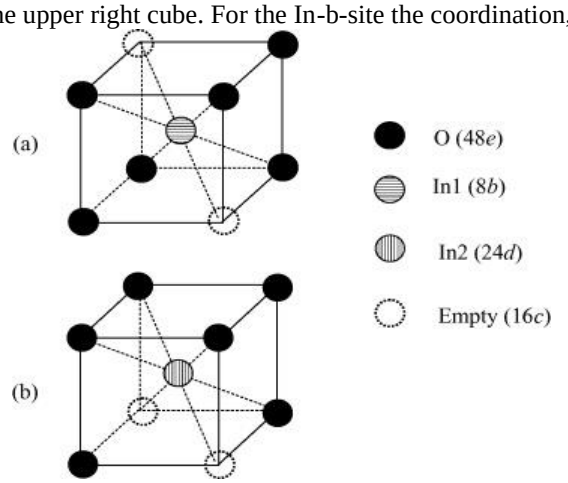

Fig. 3.1 Stick-and-ball representation of In_2O_3 crystal structures

In_2O_3-I crystallizes in a cubic bixbyite-type structure _space group No. 199_ with 8 f.u. per unit cell, with those containing three types of In and two types of O atoms occupying 8a, 12b, 12b, 24c, and 24c Wyckoff positions, respectively.

Published By:
Blue Eyes Intelligence Engineering
& Sciences Publication (BEIESP)

In Fig. 3.1, the three types of In atoms are indicated by different colors and all are surrounded by oxygen in trigonal biprism coordination. The In_2O_3-II phase also crystallizes in a cubic bixbyite-type structure with space group No. 206 and 8 f.u. per unit cell. Distinct from In_2O_3-I, it has different atomic arrangements and bond lengths, and consists of two types of In _they are surrounded by oxygen in the octahedral and trigonal prismatic coordinations alternatively, as shown in Fig. 3.1_ and one type of O atoms located at Wyckoff positions 8b, 24d, and 48e, respectively. It may be noted that the polyhedra surrounding the two types of In atoms differ from those of In_2O_3-I.

In_2O_3-III is of corundum structure with 2 f.u. per unit cell _space group No. 167_. It consists of one type of In _surrounded by oxygen in trigonal biprism coordination _ and one type of O atoms occupying 12c and 18e.

3.4 ELECTRONIC BAND STRUCTURE OF INDIUM OXIDE (In_2O_3)

For a better understanding of the electronic and optical properties and chemical bonding of the polytypes of indium oxide, the analysis of band structures can be quite helpful. Band structures for In_2O_3-I, -II, and -III calculated in this work are presented in Fig. 3.2. Although we noted above that In_2O_3-I is distorted In_2O_3-II, we still plotted band structure for both In_2O_3-I and -II to demonstrate how lattice distortion can drastically change the band structure. For example, a well distinct band region is seen in the bottom of the CB of In_2O_3-I Fig. 3.2a compared with other two polymorphs. This distinct band region is split from the rest of the CB, and it is located in the energy range 0.009–2.391 eV above the topmost valence band VB. This band region can be called as intermediate band IB. Since IB is well dispersive, recombination of electrons and holes through this band is not expected to be very high. As this band region is completely empty, it can be useful for photoemission of electrons from VB to the IB. The small difference in total energy of In2O3-I and -II and large difference in the band features at the CB minimum in these two modifications indicate that one can drastically change the optical properties by different preparatory conditions by stabilization of different proportions of these two phases.

Despite the large difference in crystal structures, In_2O_3-I, -II, and -III have some similar features. Particularly, the bottommost CB of In_2O_3-I, -II, and -III is dispersive and is located at the _ point, while the topmost VB is flat, which are the important properties inherent to TCO materials. The VB consists of three regions in all the three phases. The lowest one is located below −15 eV from the topmost VB. The bands at the intermediate energy region is located between −14 and −10 eV. Both these band energy regions are very narrow, while the topmost VB region is quite broad. The VB maximum is located at _ point for In_2O_3-I and –II and at L point for In_2O_3-III. Consequently, one can conclude that the In_2O_3-III is an indirect band gap material, while In_2O_3-I and -II are direct band gap materials.

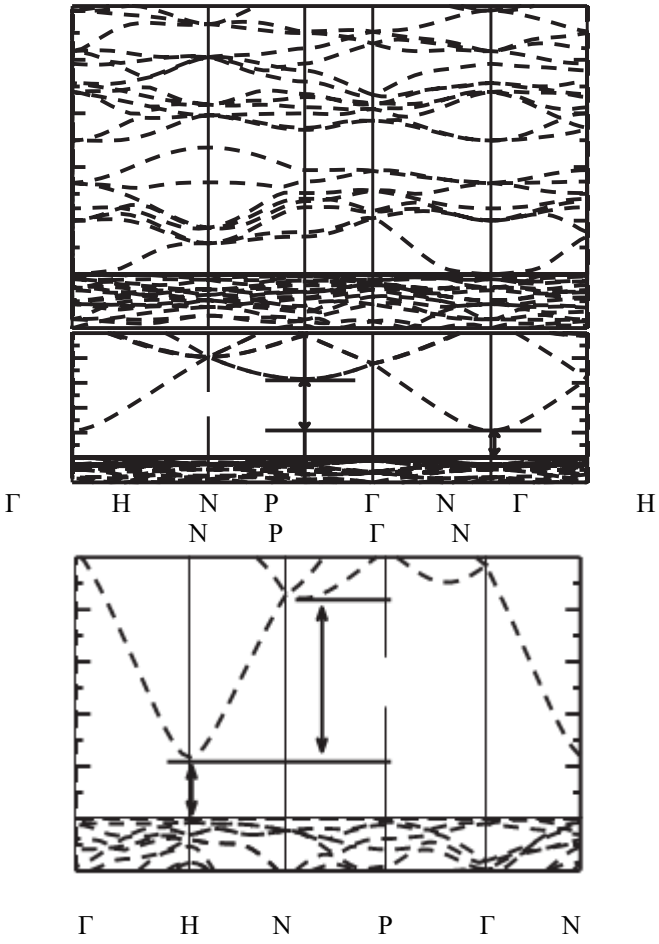

Fig. 3.2 Electronic Band structure for (a) unrelaxed In2O3-I, (b) In2O3-II, and (c) In2O3-III near the VB maximum and CB minimum. The Fermi level is set to zero.

3.5 PHYSICAL PROPERTIES OF In_2O_3

3.4.1 Optical properties

In_2O_3 is generally transparent to visible light but strongly absorbs ultra violet light below 3655 Å [127]. The absorption is typically stronger than other white pigments. In the region of visible wavelengths, regular indium oxide appears pale yellow, but, rutile and anatase titanium dioxide have a higher reactive index and thus has a superior opacity. The band gap energy (between valence and conducting bands) is 3.2 eV, this corresponds to the energy of 3655 Å photons. Under ultra violet light indium oxide is photoconductive. The combination of optical and semiconductor properties make doped indium oxide a conductor for new generations of devices. Solar cells require a transparent conductive coating, tin oxide and indium oxide (doped) are the best materials.Intrinsic optical properties of In_2O_3 nanostructures are being intensively studied for implementing photonic devices. Photoluminescence (PL) spectra of In_2O_3 nanostructures have been extensively reported. Excitonic emissions have been observed from the photoluminescence spectra of In_2O_3 nanorods. It is shown that quantum size confinement can significantly enhance the excitons binding energy [128].

Published By:
Blue Eyes Intelligence Engineering
& Sciences Publication (BEIESP)

Strong emission peak at 380 nm due to band-to-band transition andgreen-yellow emission band related to oxygen vacancy are observed. PL spectra show that In_2O_3 nanowire is a promising material for UV emission, while its UV lasing property is of more significance and interest. Due to its near-cylindrical geometry and large refractive index (~2.0), In_2O_3 nanowire/nanorod is a natural candidate for optical waveguide. The additional advantages of In_2O_3 nanowire lasers are that the excitonic recombination lowers the threshold of lasing, and quantum confinement yields a substantial density of states at the band edges and enhances radiative efficiency [129-135]. Optical waveguiding using dielectric nanowire also achieved considerable progress. Recently, In_2O_3 nanowires were reported as sub-wavelength optical waveguide. Optically pumped light emission was guided by In_2O_3 nanowire and coupled into SnO_2 nanoribbons. These findings show that In_2O_3 nanostructures can be potential building blocks for integrated optoelectronic circuit [136].

3.4.2 Chemical properties

Conductometric metal oxide semiconductor thin films are the most promising devices amongsolid state chemical sensors, due to their small dimension, low cost, low power consumption, on-line operation and high compatibility with microelectronic processing. The fundamentalsensing mechanism of metal oxide based gas sensors relies on a change in electricalconductivity due to the process of interaction between the surface complexes such as O^-, O^{-2}, H^+ and OH^- reactive chemical species and the gas molecules to be detected [137]. Many parameters are influencing the gas sensing properties such as; intrinsic surface states and extrinsic surface states. Intrinsic Surface States According to the intrinsic surface state trapping model of a temperature increase in argon atmosphere leads to a thermal excitation of valence electrons [138]. This brings them into the conduction band where they act as free charge carriers and thereby increase the electrical conductivity. The electrons in the conduction band are also thermally excited andsome may acquire enough additional energy to overcome the potential barrier at the surfaceand be trapped in unoccupied surface states. There are more electrons being trapped in a surface state than there are electrons leaving occupied surface states. Therefore the potential barrier is building up until a new thermodynamic equilibrium is established. If the sensor undergoes a quick decrease in temperature the above mentioned processis reversed. Conductance electrons will return to the valence band and occupied surfacestates will release their electrons back into the conduction band. There will be more electronsevacuating an occupied surface state than electrons being trapped into an unoccupied state. Because of this the potential barrier is lowered again to a new equilibrium [139]. The effect of a change in temperature effects the thermal excitation of an electron intoa different energy band much more quickly than the process of trapping electrons into over releasing them from surface states. Although the surface states indicate bands of energy levels it is more convenient to handle them as a single energy level E_t. To evaluate the rates for electron transfer between surfacestate E_t and conductance band E_c we assume that the rate of electron transfer is of first order.This means that (a) the rate of electron trapping is proportional to the density of unoccupied surface statesand the density of electrons in the conduction band at the surface and, (b) the rate of electron release to the conduction band is proportional to the density of occupied surface states [140].

Extrinsic Surface States Although oxygen is an oxidizing gas and could therefore be incorporated in the below section dedicated to this type of gases, it was decided to provide a full section for the discussion of O^{2-} driven surface reactions. The reason for this is that oxygen, as the dominant non-inertcomponent of air, is the reaction determining gas for measurements intended to model the influence of gases on tested gas sensors in a real-life application. At temperatures between 100-600˚C oxygen molecules in the atmosphere interact with the In_2O_3 surface. At first O_2 is adsorbed to the surface of the metal oxide through physisorption, without influencing its electric properties [141]. With the following chemisorptions and ionization the oxygen gets possibly dissociated and bound to the surface through an unoccupied chemisorption site for oxygen in molecular (O_2^-) and atomic (O^-, O^{--}) form, while extracting electrons from the semiconductor to ionize the chemisorbed oxygen. These electrons are free conduction electrons, stemming from ionized donors, which get trapped in a surface state (i.e., the chemisorbed oxygen species) and there by cannot anymore contribute to the conduction of the sensor [142-149].

3.5 Electrical properties

The values of electrical parameters of In_2O_3 thin films depend on the dopant concentration, deposition conditions and post-deposition process. The decrease in mobility with increase of dopant level is due to enhancement of scattering mechanisms such as ionized impurity scattering. The substrate temperature is found to significantly affect the electrical properties [150]. The resistivity initially decreases as the substrate temperature increases. This type of dependence of resistivity on substrate temperature may be due to the fact that crystallinity of the films improves with increase in substrate temperature, thereby increasing conductivity. At higher substrate temperatures the resistivity increases again. This increase in resistivity may be due to the oxidation of tin doped indium oxide films.The high conductivity of the In_2O_3 films has been attributed to both substitutional tin and oxygen vacancies, created either during film growth or post-deposition annealing [151]. Increasing the oxygen partial pressure above a value which yields a near stoichiometric film composition would thus result in an accumulation of excess oxygen, mainly at the grain boundaries acting as trapping centers for free carriers [152-157]. This means that the barrier scattering becomes the dominant process since the barrier height increases strongly. At the same time the density of free carriers is reduced as they are partly localized at the trapping sites [158-163]. This results in a decrease in the carrier mobility, and therefore a corresponding fall in the film conductivity is observed. Buchanan et al [164] have also suggested that the decrease in the conductivity in increased oxygen partial pressure is primarily due to a reduction in the carrier concentration caused by the occupation of oxygen vacancies rather than due to tin doping.The conductivity of In_2O_3 films can be improved by increasing the electron mobility or carrier density. There is a tradeoff between these two parameters. Very high carrier density causes strong optical absorption due to the plasma excitation of the carriers in the visible range [165].

Published By:
Blue Eyes Intelligence Engineering
& Sciences Publication (BEIESP)

Investigations on the kinetics of the crystallization of amorphous ITO and its relationship to the electrical behavior of the material during and after low temperature annealing showed that the resistivity of the material changes via two separate thermally activated processes that occur with different time constants but similar activation energies [166]. Upon heating, the as-deposited amorphous material begins to order locally via a process that obeys first order reaction rate kinetics. This change is associated with the relaxation of distorted bonds in the as-deposited amorphous material. One consequence of the local ordering that occurs during this relaxation process appears to be an increase in the ionized vacancy concentration and, consequently, the carrier density. The second stage of the transformation is crystallization via nucleation and growth with an Avrami–Johnson–Mehl growth mode parameter of 3–4, which is characteristic of two- to three-dimensional growth. This is consistent with the block-like microstructure observed by cross-sectional TEM in fully crystallized indium oxide. A more complete understanding of these processes may facilitate the development of conditions for the deposition of low resistance, high optical transmissivity indium oxide using low kinetic energy processes and low substrate temperatures.

3.6 Potential applications of In_2O_3

Due to their many appealing properties, In_2O_3 nanomaterials have been widely used in electronics [167], catalysts [168], coatings [169], and gas sensors [170] and so on, and have been a research focus for decades [171]. Amongst these applications, In_2O_3 nanoparticle based gas sensors for explosive and toxic gases are attracting more and more concern ever since the first appearance [172], due to cost effectiveness and real-time detection. Generally, much research efforts are put to use In_2O_3 nanoparticles with small sizes, which are broadly though to have high sensing sensitivity because of their large surface/volume ratio. It is also very useful in the area of energy storing materials such as; lithium ion batteries [173-180].

3.7 Fundamental methods for synthesizing nanomaterials

3.7.1 Hydrothermal/solvothermal self-assembly reaction

Hydrothermal/solvothermal reaction offers a chemical route to prepare well-defined oxide nanostructures [162-164]. The Teflon lined autoclave provides a high pressure for the accelerated chemical reaction at relatively low temperature (100–250 ˚C), which make it possible to prepare highly crystalline oxide nanostructures.

3.7.2 Spray pyrolysis

Spray pyrolysis is a synthetic route to prepare spherical oxide particles by the pyrolysis of small droplets containing cations at high temperature. Nozzle and ultrasonic transduction are used to produce aerosols in the order of several micrometers. If the solvent evaporates rapidly or the solubility of the source materials is low, local precipitation occurs near the droplet surface, which leads to the formation of hollow spheres [165-168]. In order to prepare hollow spheres by spray pyrolysis, droplets with a short retention time at high temperature are desirable to attain the high super saturation at the droplet surface prior to the evaporation of the entire solvent. Usually, no templates are necessary to produce hollow structures in spray pyrolysis.

We are using the following method;

Co-Precipitation Method: The nanocrystalline powder of Sn-doped In_2O_3 was prepared by controlled co-precipitation technology. A diluted ammonia hydroxide solution was used to hydrolyze the metal salt precursors at a certain solution pH value. The metal salts of $SnCl_4 \cdot 5H_2O$ and $InCl_3 \cdot 4H_2O$ were dissolved in distilled water at a total metal cation concentration (Sn^{4+} + In^{3+}) varying from 0.01M to 0.2 M. Polyaniline polymer added to the above solution, after that ammonium hydroxide was added drop wise to the solution until the final solution pH value of about 7.8. Following precipitation, the slurry was aged for 24 h, and then draw filtrated, washed three to four times with distilled water to remove the chloride ions, dried at 100–120 ºC and ground into a powder which is the precursor. The precursors were calcined in air at different temperatures of 400 ºC for 4 h to produce composite nanocrystalline powders with different grain size. In this co-precipitation method, the precipitation pH value was a critical preparation parameter. Intermediate pH values of 8 ensured that both components would precipitate simultaneously to form homogeneous nanocomposites. If the pH value was raised above 9, the precipitated $Sn(OH)_4$ re-dissolved, and the optimal precipitation pH value was thus about 7.8. Other processing parameters, such as metal salt concentration, the In/Sn ratio, aging time and calcination temperature, were also investigated and determined to control the grain size and crystallinity of the nanocomposites derived [169].

3.8 Characterization Techniques

3.9 3.8.1 X-ray diffraction technique

3.10 The formation of crystal phases in the synthesized samples was investigated by performing the X-ray diffraction measurements at room temperature. The XRD measurements on powder samples were performed with the XPERT-PRO (PW3050/60) equipped with Cu-Kα radiation (λ = 1.54060 Å) operated at 30 kV and 30 mA [170-174]. Samples were scanned in the angle range of 10–80º with a scanning rate of 0.1 (degree) / min. A digital photograph of X-ray diffractometer is shown in Fig. 3.2.

Fig. 3.2: Digital photograph of X-ray diffractometer

3.10.2 Ultra-Violet Visible spectrophotometer (UV-VIS. spectrophotometer)

UV-Visible spectra of the prepared samples were recorded in the range of 200–800 nm using Hitachi 330 UV-VIS spectrometer for optical band gap calculations. The instrument has an integrating sphere to analyze the powder form of the samples in the range of 200-800 nm and a specular reflectance accessory for studying the reflective surfaces [175-178].

A digital photograph of UV-Vis spectrometer is shown in Fig. 3.3.

Fig. 3.3: Digital photograph of UV-Vis spectrometer.

3.11 Objective and scope of present work

Monitoring all aspects of the environment in real time has been one of the key requirements of the last decades, and this in turn led to a great effort in terms of research and funding for the development of all kind of sensors. Chemical sensors are in the research focus from several years due the increasing concerns for pollution and its effects on health and safety. Concerning metal oxides chemical sensors, it is well known from six decades that their electrical conductivity varies with the surrounding atmosphere. Several studies of the sensing properties of semiconductor metal oxides in form of thin or thick films and pellets have been reported in literature. In_2O_3 is the promising materials for gas sensing applications. The formaldehyde is a colorless, pungent-smelling gas, and usually used as a regent for adhesives such as urea-formaldehyde (UF) and phenol-formaldehyde (PF) resins. It is considered as the most serious indoor contamination at new house because those regents with formaldehyde are widely applied in fabricating furniture and decorating house. To date, the detection of formaldehyde is taken on by the cataluminescence [179], spectroscopy [180], chemiresistor and bio-sniffer, etc. These detection devices need either the high temperature operation or huge equipment, high cost. The detection of formaldehyde gas based on the In_2O_3 gas sensor is a novel approach, which can overcome those defects of detection technologies developed.

III. RESULTS AND DISCUSSION

4.1 Structural and morphological characterizations

Fig. 4.1 represent the X-ray diffraction (XRD) spectra of polymer embedded the undoped and Sn-doped In_2O_3 nanoparticles synthesized by co-precipitation method. All peaks may be well matched with the cubic In_2O_3 (JCPDS card no. 06-0416), indicating high purity and crystallinity. It has been observed in the figure 4.1 that the samples are polycrystalline in nature, possessing cubic structure. It is also found that there is no impurity phase corresponding to Sn [181-186].

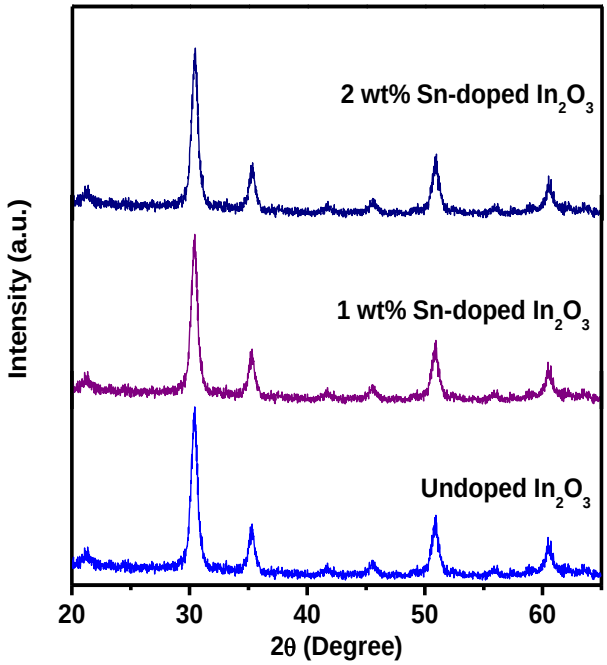

Fig. 4.1: X-ray diffraction patterns of the polymer embedded undoped and Sn-doped In_2O_3 nanoparticles.

The crystallite size D is calculated using the Scherrer formula [187-190].

$D=0.9\lambda/\beta\cos\theta$ ….. (4.1)

$\varepsilon=\beta/4\tan\theta$ ……. ….. (4.2)

where λ is the wavelength of the incident X-ray (λ = 1.5418 Å), β is the full width at half maximum (FWHM), in radians, of the maximum intensity peak, ε is the lattice strain and θ is the angle at which the maximum peak occurs. The calculated crystallite sizes and strains are ~43, ~35, ~29 nm and 0.0085, 0.0097 and 0.0105 respectively. It is found that as Sn doping increases, the peak intensity of the samples slightly increases. This may be due to the creation of more crystallites corresponding to that plane.

It is also shown in Figure 4.1 that the peaks shifted towards lower Bragg's angle side. This may be due different ionic radii of In and Sn. It is well known that for incorporation of any dopant, the ionic radii of the dopant and the host lattice must not differ by more than 15%. In the present case, the ionic radii of In^{3+} and Sn^{4+} are 0.74 and 0.69 Å, respectively, and therefore substitution of Sn^{4+} ions in place of In^{3+} ions is possible in the In_2O_3 structure. It is observed that as Sn doping concentration increases crystallite size decreases. This is attributed to fact that density of nucleation center increases [191-199].

Fig. 4.2 show the scanning electron microscopy (SEM) images of the polymer embedded undoped and Sn-doped In_2O_3 nanoparticles. These SEM images show the flakes shape in undoped sample and agglomerated Sn-doped In_2O_3 nanoparticles. The agglomeration of particles on the polymer matrix may be due the different surface energy of the solvent [200-205].

Published By:
Blue Eyes Intelligence Engineering
& Sciences Publication (BEIESP)

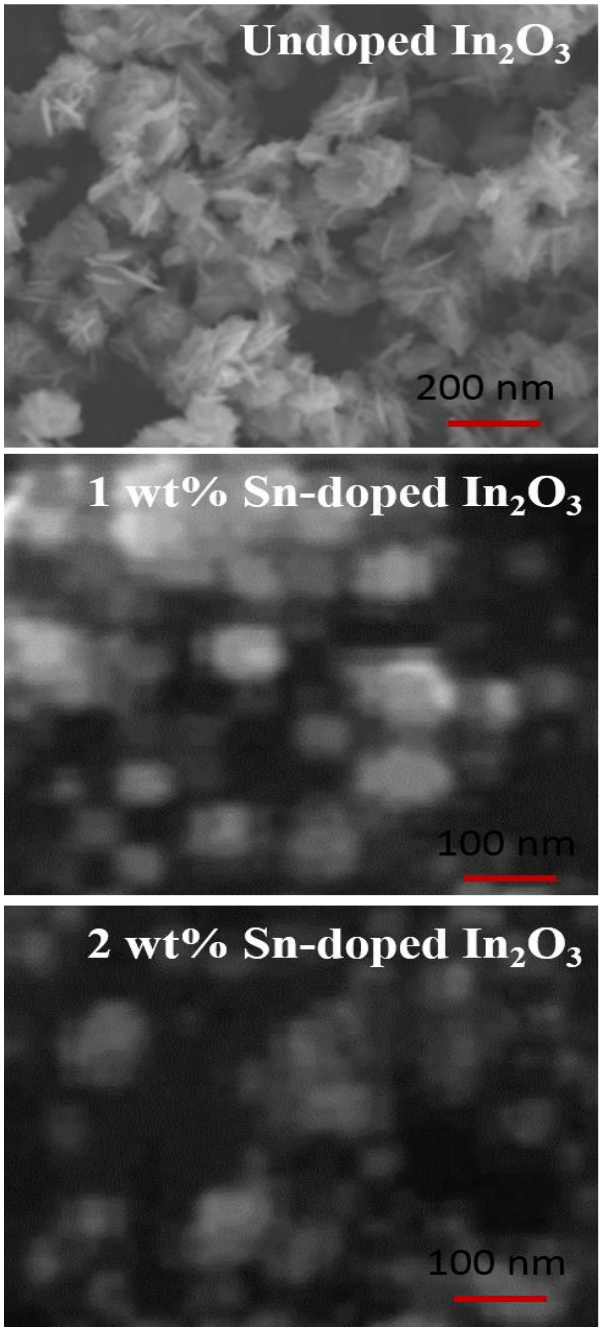

Fig. 4.2 Show the SEM micrographs of the polymer embedded undoped and Sn-doped In_2O_3 nanoparticles.

4.2 Optical studies

The optical band gap of polycrystalline polymer embedded undoped and Sn-doped In_2O_3 nanoparticles were calculated from the optical absorption study. The optical absorption is related to the band gap of a semiconductor, which satisfies the equation 4.3 [206-207].

$$\alpha = k(h\nu - E_g)^{1/2} \quad \ldots\ldots\ldots\ldots\ldots \quad (4.3)$$

where A is a constant, E_g is the optical band gap and hν is the incident photon energy.

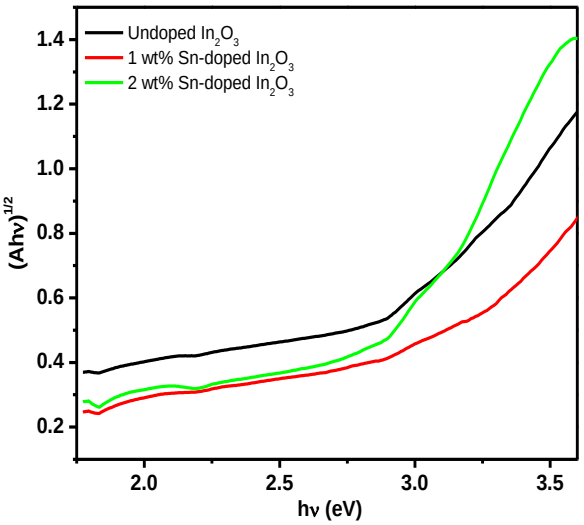

Fig. 4.3: Optical band gap calculation of the polymer embedded undoped and Sn-doped In_2O_3 samples.

Plots of lnα vs. hν showing straight line fits indicate that the In_2O_3 prepared in the present work are direct band gap semiconductors.

The band gap can be estimated from the Tauc plot of $(\alpha h\nu)^2$ versus hν (photon energy) by extrapolating the linear part of the plot to the energy axis. Fig. 4.3 indicates the optical band gap spectra of the undoped and Sn-doped In_2O_3 nanoparticles. It is observed that Sn doping influences the optical bad gap of the In_2O_3 samples. The estimated optical band gap of the undoped and Sn-doped In_2O_3 samples are 3.60 eV, 3.64 eV and 3.90 eV. The Sn doping modified optical band gap may be due to lattice strain or due to the polymer effects [208-209].

The localized states (E_o) in the energy band gap, commonly called the Urbach tail has been estimated with help of linear extrapolating lnα vs hν graph and found to be 0.510 eV, 0.653 eV and 0.807 eV for the undoped and Sn-doped In_2O_3 samples. It is observed that as crystallite size decreases band gap increases, therefore localized energy states increases [210].

3.2 Electrical studies

The variation of the resistance of the undoped and Sn-doped In_2O_3 nanoparticles for operating temperature range 100-300°C have been measured. The behaviour of the electrical conductivity and the activation energies have been carried out.

3.2.1 Electrical conductivity studies

The variation of conductivity of the undoped and Sn-doped In_2O_3 nanoparticles is shown in Fig. 4.4. Figure shows that for all temperature range conductivity found be increases. This is attributed due to the fact that thermal excitation of electrons from the valance band to the conduction band.

The change in conductivity of the undoped and Sn-doped In_2O_3 was measured in the temperature range 100–300°C, by applying a dc. 10V bias across the pellets having silver contact of both faces to maintain conductive samples. The experimental data so obtained has been used to calculate the activation energy using the formula [211]:

$$\sigma=\sigma_o\exp(-\Delta E_a/kT) \quad \ldots\ldots \quad (4.4)$$

…..

(4.4)

where ΔE_a is the activation energy which corresponds to the energy difference between the valance band and the conduction band, σ_o is a temperature independent factor and k is the Boltzmann's constant and T is the absolute temperature.

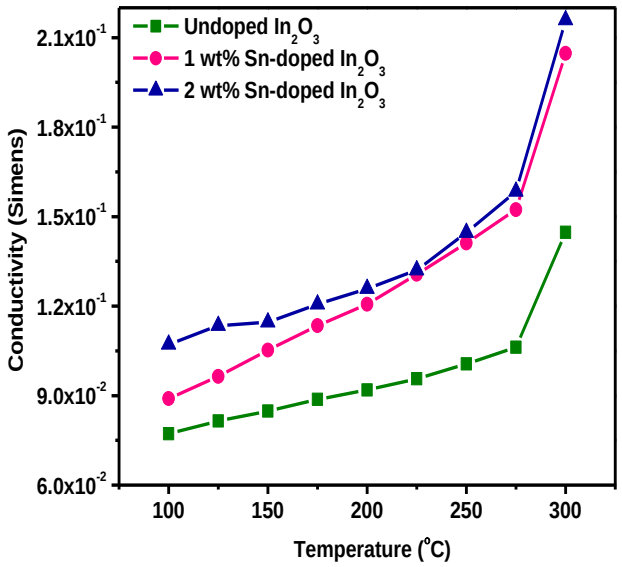

Fig. 4.4: Shows electrical conductivity of polymer embedded undoped and Sn-doped In_2O_3 nanoparticles.

Fig. 4.5 represents the ln σ vs. 1/T curves for undoped and Sn-doped In_2O_3 nanoparticles synthesized by co-precipitation method. It is seen that the conductivity increases with temperature indicating, the semiconducting behaviour of the samples and suggesting a thermally activated conduction mechanism. From the slope of plots in Fig. 4.5, the activation energy for undoped and Sn-doped In_2O_3 nanoparticles are calculated. The activation energy of the undoped and Sn-doped In_2O_3 nanoparticles is 0.02013 eV, 0.00473 eV and 0.0065 eV, respectively. The decrease in activation energy with increase in Sn-doping concentration can be understood from the less scattering between grains. The growth of grains with dopant concentration leads to reduction in grain boundary scattering thus increases the samples conductivity [212-215].

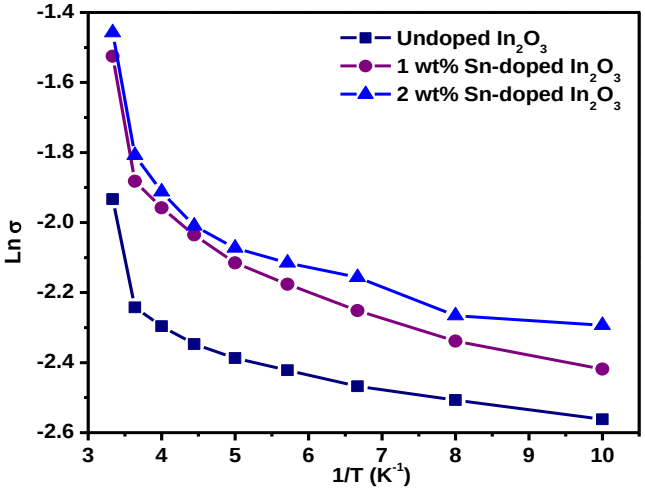

Fig. 4.5: Shows Arrhenius plot for the calculation of activation energy of polymer embedded undoped and Sn-doped In_2O_3 nanoparticles.

IV. CONCLUSIONS AND FUTURE SCOPE THE WORKCONCLUSIONS

The following points are concluded from the whole project work;

1. Nanotechnology is sometimes referred to as a general purpose technology because in its advanced version it will have significant impact on almost all industries and all areas of society.
2. Nanotechnology has been subject to numerous discussions and developments during last few decades, starting from Richard Feynman's speech in 1959, followed by the introduction of the word "Nanotechnology" in 1974 by Norio Taniguchi.
3. The literature review on the In_2O_3 nanoparticles have been discussed many scenarios which give the importance of the human beings. Therefore, authors project work based on energy storing materials.
4. The literature provides the importance and many applications of In_2O_3. Therefore, authors have been investigated the structural, optical and electric properties of the undoped and Sn-doped In_2O_3 nanoparticles.
5. Conducting polymer and their composites have attracted the attention of material researchers extensively, because of their wide spread applications in organic light emitting diodes (OLED).
6. In order to avoid such problems, all electronic equipments must be shielded against electromagnetic aggressions. Composites based on polymers, like hexagonal-ferrite/polymer, metal/metal oxide polymer composites, and single wall carbon nanotube–epoxy composites.
7. Indium oxide (In_2O_3) is a technologically important transparent conducting oxide (TCO) material. Indium oxide is an n-type semiconductor with wide energy band gap in the range of 3.60-3.72.
8. The structure of In_2O_3 in its crystalline form is body centered cubic (bcc) with a lattice constant of about 10.11 Å.
9. High optical transparency in the visible region more than 80%, low electrical resistivity less than 10^{-3} Ωcm and high infrared reflectivity make indium oxide (In_2O_3) a choice for many potential applications in the upcoming nanoelectronic building blocks.
10. In_2O_3 shows interesting and technologically important combination of properties viz. high luminous transmittance, high IR reflectance, good electrical conductivity, excellent substrate adherence and chemical inertness.
11. Beyond these key properties of transparent conducting oxides (TCOs), In_2O_3 has a number of other key characteristics. The structure of In_2O_3 can be amorphous, crystalline, or mixed, depending on the deposition temperature and atmosphere.
12. In general, In_2O_3 deposited at room temperature is amorphous, and In_2O_3 deposited at higher temperatures is crystalline. Depositing at high temperatures is more expensive than at room temperature, and this method may not be compatible with the underlying devices.

Published By:
Blue Eyes Intelligence Engineering
& Sciences Publication (BEIESP)

13. TCOs on window glass improve the energy efficiency of the window because free electrons reflect infrared radiation for wavelengths longer than the plasma wavelength. In cold climates, the plasma wavelength of about 2μm is desirable, so that most of the solar spectrum is transmitted to heat inside the building.
14. An XRD result confirms the body centered cubic (bcc) structure of the undoped and Sn-doped In_2O_3 nanoparticles, there is no other phase was found corresponding to Sn.
15. The crystallite sizes and strains for undoped and Sn-doped In_2O_3 nanoparticles have been found ~43 nm, ~35 nm ~29 nm 0.0085, 0.0097 and 0.0105 respectively.
16. SEM provides the morphological studies of the undoped and Sn-doped In_2O_3 nanoparticles which is in spherical in shape and agglomerated nanoparticles.
17. It is observed that Sn doping influences the optical bad gap of the In_2O_3 samples. The estimated optical band gap of the undoped and Sn-doped In_2O_3 samples are 3.60 eV, 3.64 eV and 3.90 eV.
18. The localized states (E_o) in the energy band gap, commonly called the Urbach tail has been estimated with help of linear extrapolating lnα vs hν graph and found to be 0.510 eV, 0.653 eV and 0.807 eV for the undoped and Sn-doped In_2O_3 samples.
19. It is seen that the conductivity increases with temperature indicating, the semiconducting behaviour of the samples and suggesting a thermally activated conduction mechanism.
20. The activation energy of the undoped and Sn-doped In_2O_3 nanoparticles is 0.02013 eV, 0.00473 eV and 0.0065 eV, respectively.
21. The decrease in activation energy with increase in Sn-doping concentration can be understood from the less scattering between grains.
22. At higher operating temperatures the thermal energy obtained is high enough to overcome the potential barrier and thus the electron concentration increases, which in turn leads to an increase in charge holding capacity of the polymer embedded undoped and Sn-doped In_2O_3 system.
23. The Sn-doping affects the energy storage and loss capacity of the In_2O_3 system. Therefore, we can say that Sn-doped In_2O_3 nanoparticles may be good material for energy storing devices.

Future Scope the Work:

Future Impact of this work:

Taking account for the increasing issues on the future energy materials. The present work has been carried out on this issue. The impact of this work is to offer some understanding of the microscopic effects of doping and correlate these effects with the macroscopic properties of In_2O_3. This work addresses fundamental issues of energy storing pertaining to Sn-doping of In_2O_3 based devices and proposes solutions to tackle these issues.

REFERENCES

1. A. Bagheri khatibani, A. Abdolahzadeh Ziabari, S. M. Rozati and Z. Bargbidi and G. Kiriakidis, Characterization and Gas-sensing Performance of Spray pyrolysed In_2O_3 Thin Films: Substrate Temperature Effect, Transactions On Electrical And Electronic Materials, Vol. 13, No. 3, pp. 111-115, June 25, 2012.
2. V. Brinzari, G. Korotcenkov, V. Matolin, Synchrotron radiation photoemission study of indium oxide surface prepared by spray pyrolysis method, Appl. Surf. Sci. 243 (2005) 335–344.
3. G. Korotcenkov, V. Brinzari, A. Cerneavschi, M. Ivano, A. Cornet, J. Morante, A. Cabot, J. Arbiol, In2O3 films deposited by spray pyrolysis: gas response to reducing (CO, H_2) gases, Sens. Actuators B 98 (2004) 122–129.
4. Nanotechnology: A Brief Literature Review M. Ellin Doyle, Ph.D Food Research Institute, University of Wisconsin–Madison, Madison, WI 53706.
5. Research Strategies for Safety Evaluation of Nanomaterials, Part IV: Risk Assessment of Nanoparticles.
6. P. Prathap, G. Gowri Devi, Y.P.V. Subbaiah, K.T. Ramakrishna Reddy, V. Ganesan, Growth and characterization of indium oxide films, Current Appl. Phys. 8 (2008) 120–127.
7. A. Teeramongkonrasmee, M. Sriyudthsak, Methanol and ammonia sensing characteristics of sol–gel derived thin film gas sensor, Sens. Actuators B 66 (2000) 256–259.
8. Gajjar P, Pettee B, Britt DW, Huang W, Johnson WP, Anderson J. Antimicrobial activities of commercial nanoparticles against an environmental soil microbe, Pseudomonas putida KT2440. Journal of Biological Engineering. 2009, 3:9-22.
9. Feynman R. There's plenty of room at the bottom. Science. 1991, 254:1300-1301.
10. Parak WJ, Gerion D, Pellegrino T, Zanchet D, Micheel C, Williams CS, Boudreau R, Le Gros MA, Larabell CA, Alivisatos AP: Biological applications of colloidal nanocrystals. Nanotechnology. 2003,14:15-27.
11. Whitesides GM. The 'right' size in Nanobiotechnology. Nature Biotechnology. 2003, 21:1161-1165.
12. Gutierrez FM, Olive PL, Banuelos A, Orrantia E, Nino N, Sanchez EM, Ruiz F, Bach H, Gay YA. Synthesis, characterization, and evaluation of antimicrobial and cytotoxic effect of silver and titanium nanoparticles. Nanomedicine, 2010, 6:681-688.
13. Eustis S, El-Sayed MA. Why gold nanoparticles are more precious than pretty gold: Noble metal surface plasmon resonance and its enhancement of the radiative and nonradiative properties of nanocrystals of different shapes. Chemical Society Reviews, 2006, 35:209-217.
14. Gupta AK, Gupta M. Synthesis and surface engineering of iron oxide nanoparticles for biomedical applications, Biomaterials. 2005; 26:3995-4021.
15. Jamieson T, Bakhshi R, Petrova D, Pocock R, Imani M, Seifalian AM. Biological applications of quantum dots, Biomaterials.2007; 28: 4717-4732.
16. Samia ACS, Dayal S, Burda C. Quantum dot-based energy transfer: Perspectives and potential for applications in photodynamic therapy. Photochemistry and Photobiology. 2006; 82:617-625.
17. Dunn K, Edwards-Jones V. The role of Acticoat with nanocrystalline silver in the management of burns. Burns. 2004; 30:1–9.
18. Russell AD, Hugo WB. Antimicrobial activity and action of silver. Prog. Med. Chem. 1994; 31:351-370.
19. Ip M, Lui SL, Poon VK, Lung I, Burd A. Antimicrobial activities of silver dressings: an in vitro comparison. J Med Microbiol. 2006; 55:59–63.
20. Petica A, Gavriliu S, Lungu M, Buruntea N, Panzaru C. Colloidal silver solutions with antimicrobial properties. Mater Sci Eng. 2008; 152:22–27.
21. Foley, E., & Hersam, M. (2006). Assessing the need for nanotechnology education reform in the United States. Nanotechnology Law and Business, 3, 467–484.
22. Greczylo, T., & Debowska, A. (2006). The macroscopic model of an atomic force microscope in the students' laboratory. European Journal of Physics, 27, 501–513.
23. Jones, M.G., Tretter, T., Taylor, A., & Oppewal, T. (2008). Experienced and novice teachers' concepts of spatial scale. International Journal of Science Education, 30, 409–429.
24. Jayanta Kumar Behera, Synthesis and Characterization of Nano-particles. M.Tech Thesis, NIT Rourkela.
25. http://www.znoxide.org/properties.html Physical Properties of Zinc Oxide - CAS 1314-13-2 International Zinc Association. http://wiki.verkata.com/en/wiki/Nanoparticle, Nanoparticle.
26. B. C. Yadav, Richa Srivastava and Alok Kumar.Characterization of ZnO Nanomaterial Synthesized by dierent methods. International Journal of Nanotechnology and Applications, 2007, volume1.
27. Taylor, A., & Jones, G. (2009). Proportional reasoning ability and concepts of scale: Surface area to volume relationship in science. International Journal of Science Education, 31, 1231–1247.

28. Tomasik, J., Jin, S., Hamers, R., & Moore, J. (2009). Design and initial evaluation of an online nanoscience course for teachers. Journal of Nano Education, 1, 48–69.
29. Toumey, C., & Baird, D. (2008). Nanoliteracy: Nurturing understandings of nanotechnology and societal interactions with nanotech. In A.E. Sweeney & S. Seal (Eds.), Nanoscale science and engineering education (pp. 577–589). Valencia CA: American Scientific Publishers.
30. Jun Tamaki, Chizuko Naruo, Yoshifumi Yamamoto, Masao Matsuoka, Sensing properties to dilute chlorine gas of indium oxide based thin film sensors prepared by electron beam evaporation, Sens. Actuators B 83 (2002) 190-194.
31. Wan-Young Chung, , Go Sakai, Kengo Shimanoe, Norio Miura, Duk-Dong Lee, Noboru Yamazoe, Spin-coated indium oxide thin film on alumina and silicon substrates and their gas sensing properties, Sens. Actuators B 65 (2000) 312–315.
32. R. Winter, K. Scharnagl, A. Fuchs, T. Doll, I. Eisele, Molecular beam evaporation-grown indium oxide and indium aluminium films for low-temperature gas sensors, Sens. Actuators B 66 (2000) 85–87.
33. M. Suchea, N. Katsaraki, S. Christoulakis, S. Nikolopoulou, G. Kiriakidis, Low temperature indium oxide gas sensors, Sens. Actuators B 118 (2006) 135–141.
34. P.P. Edwards, J.M. Thomas, Angew. Chem. Int. Ed. 46 (2007) 5480.
35. J.H. Liebarth, R.H. Persellin, Agents. Actions. 11 (1981) 458.
36. I.M. Rutkow, The History of Surgery in the United States, 1775-1900, Jeremy Norman Co, 1988.
37. N. Krause, N. Morita, in: R.H. Crabtree, D.M.P. Mingos (Eds.), Comprehensive Organometallic Chemistry III, Elsevier, Oxford, 2006. http://www.aadet.com/article/nanoparticle, Nanoparticle Data.
38. H.H. Helcher, Aurum Potabile oder Gold Tinstur, J. Herbord Klossen, Breslau and Leipzig, 1718. http://www.scribd.com/doc/43567667/Next-Generation-Technology-1
39. F. Antonii, Panacea Aurea-Auro Potabile, Bibliopolio Frobeniano, Hamburg, 1618. http://www.coursehero.com/le/1344664/JianLiTIP06/.
40. G. Savage, Glass and Glassware, Octopus Book, London, 1975.
41. http://www.reachinformation.com/de ne/nanoparticle.aspx Nanoparticles.
42. P.H. Howard, Handbook of Environmental Fate and Exposure Data for Organic Chemicals, Lewis Publishers, Chelsea, MI, 1991.
43. W.H. Ahrens (Ed.), Herbicide Handbook: Weed Science Society of America, Allen Press, Lawrence, USA, 1994.
44. Y.I. Korpan, M.V. Gonchar, A.A. Sibirny, C. Martrlet, A.V. El'skaya, T.D. Gibson, A.P. Soldatkin, Development of highly selective and stable potentiometric sensors for formaldehyde detection, Biosens. Bioelectron. 15 (2000) 77–83.
45. R. Kataky, M.R. Bryce, L. Goldenberg, S. Hayes, A. Novak, A biosensor for monitoring formaldehyde using a new lipophilic tetrathiafulvalene-tetracyanoquino dimethane salt and a polyurethane membrane, Talanta 56 (2002) 451–458.
46. P.A. Buffat, J.-P. Borel, Phys. Rev. A 13 (1976) 2287.
47. J.-S. Hu, L.-S. Zhong, W.-G. Song, L.-J. Wan, Synthesis of hierarchically structured metal oxides and their application in heavy metal ion removal, Adv. Mater. 90 (2008) 2977–2982.
48. A.-M. Cao, J.-S. Ju, H.-P. Liang, W.-G. Song, L.-J. Wan, X.-L. He, X.-G. Gao, S.-H. Xia, Hierarchically structured cobalt oxide (Co3O4): the morphology control and its potential in sensors, J. Phys. Chem. B. 110 (2006) 15858–15863.
49. L. Zhang, W. Wang, Z. Chen, L. Zhou, H. Xu, W. Zhu, Fabrication of flower-like Bi2WO6 superstructures as high performance visible-light driven photocatalysts, J. Mater. Chem. 17 (2007) 2526–2532.
50. H. Xu, Z. Zheng, L. Zhang, H. Zhang, F. Deng, Hierarchical chlorine-doped rutile TiO_2 spherical clusters of nanorods: large-scale synthesis and high photocatalytic activity, J. Solid State Chem. 181 (2008) 2516–2522.
51. S. Sun, W. Wang, H. Xu, L. Zhou, M. Shang, L. Zhang, $Bi_5FeTi_3O_{15}$ hierarchical microflowers: hydrothermal synthesis, growth mechanism, and associated visible-light-driven photocatalysts, J. Phys. Chem. C 112 (2008) 17835–17843.
52. E. Hosono, S. Fujihara, I. Honma, M. Ichihara, H.S. Zhou, Fabrication of nano/micro hierarchical Fe2O3/Ni micrometer-wire structure and characteristics for high rate Li rechargeable battery, J. Electrochem. Soc. 153 (2006) A1273–A1278.
53. S. Sun, G. Meng, G. Zhang, J.P. Masse, L. Zhang, Controlled growth of SnO_2 hierarchical nanostructures by amultistep thermal vapor deposition process, J. Eur. Chem. 13 (2007) 9087–9092.
54. Q.Wang, K. Yu, F. Xu, Synthesis and filed emission of two kinds of hierarchical SnO_2 nanostructures, Solid State Commun. 143 (2007) 260–263.
55. L. Qin, J. Xu, X. Dong, Q. Pan, Z. Cheng, Q. Xiang, F. Li, The template-free synthesis of square-shaped SnO2 nanowires: the temperature effect and acetone gas sensors, Nanotechnology 19 (2008) 185705.
56. J.A. Bumpus, M. Tien, D. Wright, S.D. Aust, Science 228 (1985) 1434. D. Voet, J.G. Voet, Biochemistry – Biomolecules, Mechanisms of Enzyme action, and Metabolism, John Wiley and Sons, Inc, New Jersey, 2004.
57. E.A. Hauser, J.E. Lynn, Experiments in Colloid Chemistry, McGraw Hill, New York NY, 1940.
58. G. Soncini, Potentiometric detection of formaldehyde in air by an aldehyde dehydrogenase FET, Sens. Actuators B 37 (1996) 49–54.
59. Y. Mine, N. Melander, D. Richter, D.G. Lancaster, K.P. Petrov, R.F. Curl, F.K. Tittel, Detection of formaldehyde using min-infrared difference-frequency generation, Appl. Phys. B 65 (1997) 771–774.
60. R. Knake, P. Jacquinor, P.C. Hauser, Amperometric detection of gaseous formaldehyde in the ppb range, Electroanalysis 13 (2001) 631–634.
61. M. Hämmerle, E.A.H. Hall, N. Cade, D. Hodgins, Electrochemical enzyme sensor for formaldehyde operating in the gas phase, Biosens. Bioelectron. 11 (1996) 239–246.
62. S. Friedfeld, M. Fraser, D. Lancaster, D. Leleux, D. Rehle, F. Tittel, Field inter comparison of a novel optical sensor for formaldehyde quantification, Geophys. Res. Lett. 27 (2000) 2093–2096.
63. R.L. Bunde, E.J. Jarvi, J.J. Rosebtreter, A piezoelectric method for monitoring formaldehyde induced crosslink formation between poly-lysine and polydeoxyhuanosine, Talanta 51 (2000) 159–171.
64. Y. Shimizu, T. Maekawa, Y. Nakamura, M. Egashira, Effects of gas diffusivity and reactivity on sensing properties of thick film SnO2-based sensors, Sens. Actuators B 46 (1998) 163–168.
65. N. Yamazoe, Toward innovations of gas sensor technology, Sens. Actuators B 108 (2005) 2–14.
66. J.H. Lee, Gas sensors using hierarchical and hollow oxide nanostructures: overview, Sensors and Actuators B 140 (2009) 319–336.
67. H. Zhang, Q. Zhu, Y. Zhang, Y. Wang, L. Zhao, B. Yu, One-pot synthesis and hierarchical assembly of hollow Cu2O microspheres with nanocrystals-composed porous multi shell and their gas-sensing properties, Advanced Functional Materials, 17 (2007) 2766–2771.
68. W. Guo, T. Liu, H. Zhang, R. Sun, Y. Chen, W. Zeng, Z. Wang, Gas-sensing performance enhancement in ZnO nanostructures by hierarchical morphology, Sensors and Actuators B 166–167 (2012) 492–499.
69. H. Liang, H. Zhang, J. Hu, Y. Guo, L. Wan, C. Bai, Pt hollow nanospheres: facile synthesis and enhanced electrocatalysts, Angewandte Chemie International Edition 43 (2004) 1540–1543.
70. S.W. Kim, M. Kim, W.Y. Lee, T. Hyeon, Fabrication of hollow palladium spheres and their successful application to the recyclable heterogeneous catalyst for suzuki coupling reactions, Journal of the American Chemical Society 124 (2002) 7642–7643.
71. Y. Zhu, T. Ikoma, N. Hanagata, S. Kaskel, Rattle-type Fe3O4@SiO2 hollow mesoporous spheres as carriers for drug delivery, Small 6 (2010) 471–478.
72. W. Wei, G. Ma, G. Hu, D. Yu, T. McLeish, Z. Su, Z. Shen, Preparation of hierarchical hollow $CaCO_3$ particles and the application as anticancer drug carrier, Journal of the American Chemical Society 130 (2008) 15808–15810.
73. D. Grosso, C. Boissiere, C. Sanchez, Ultralow-dielectric-constant optical thin films built from magnesium oxyfluoride vesicle-like hollow nanoparticles, Nature Materials 6 (2007) 572–575.
74. S.C. Yang, D.J. Yang, J. Kim, J.M. Hong, H.G. Kim, I.D. Kim, H. Lee, hollow TiO_2 hemispheres obtained by colloidal templating for application in dye-sensitized solar cells, Advanced Materials 20 (2008) 1059–1064.
75. A. Cao, J. Hu, H. Liang, L. Wan, Self-assembled vanadium pentoxide (V_2O_5) hollow microspheres from nanorods and their application in lithium-ion batteries, Angewandte Chemie International Edition 44 (2005) 4391–4395.
76. X. Lou, L. Archer, Z. Yang, Hollow micro-nanostructures: synthesis and applications, Advanced Materials 20 (2008) 3987–4019.
77. P. Sun, W. Zhao, Y. Cao, Y. Guan, Y. Sun, G. Lu, Porous SnO_2 hierarchical nanosheets: hydrothermal preparation, growth mechanism, and gas sensing properties, Cryst Eng Comm 13 (2011) 3718–3724.

Published By:
Blue Eyes Intelligence Engineering
& Sciences Publication (BEIESP)

78. B. Liu, H. Zeng, Hollow ZnO microspheres with complex nanobuilding units, Chemistry of Materials 19 (2007) 5824–5826.
79. R. Gutierrez-Osuna, Pattern analysis for machine olfaction: a review, IEEE Sensors Journal 2 (3) (2002).
80. C. Distante, M. Leo, P. Siciliano, K. Persaud, On the study of feature extraction methods for an electronic nose, Sensors and Actuators B 87 (2002) 274–288.
81. K. Jain, R.P.W. Duin, M. Jianchang, Statistical pattern recognition: a review, IEEE Transactions on Pattern Analysis and Machine Intelligence 22 (1) (2000).
82. A. Webb, Statistical Pattern Recognition, Arnold, London UK, 1999, xviii+454 pp., ISBN 0-340-74164-3.
83. C. Bishop, Neural Networks for Pattern Recognition, Oxford University Press, 1995.
84. M. Santonico, G. Pennazza, R. Capuano, C. Falconi, T.J. Vink, H.H. Knobel, A. D'Amico, Electronic noses calibration procedure in the context of a multicenter medical study, Sensors and Actuators B: Chemical 173 (2012) 555–561.
85. G. Sberveglieri, I. Concina, E. Comini, M. Falasconi, M. Ferroni, V. Sberveglieri, Synthesis and integration of tin oxide nanowires into an electronic nose, Vacuum 86 (2012) 532–535.
86. E. Comini, G. Faglia, M. Falasconi, M. Ferroni, M. Pardo, G. Sberveglieri, Odour unit quantification in landfill by an innovative electronic nose based on metal oxide thin films, in: C.L. Ernest (Ed.), Landfill Research Focus, Nova Science Publishers, Hauppauge NY, USA, 2010, pp. 117–134.
87. M. Peris, L. Escuder-Gilabert, A 21st century technique for food control: electronic noses, Analytica Chimica Acta 638 (1) (2009) 1–15.
88. L.M. Reid, C.P. O'Donnell, G. Downey, Recent technological advances for the determination of food authenticity, Trends in Food Science and Technology 17 (7) (2006) 344–353.
89. E. Schaller, J.O. Bosset, F. Escher, 'Electronic noses' and their application to food, Sensors and Actuators B: Chemical 31 (4) (1998) 305–316.
90. M. Ghasemi-Varnamkhasti, S. Saeid Mohtasebi, M. Siadat, Biomimetic-based odor and taste sensing systems to food quality and safety characterization: an overview on basic principles and recent achievements, Journal of Food Engineering 100 (2010) 377–387.
91. A. Berna, Metal oxide sensors for electronic noses and their application to food analysis, Sensors 10 (2010) 3882–3910, http://dx.doi.org/10.3390/s100403882.
92. N. El Barbri, J. Mirhisse, R. Ionescu, N. El Bari, X. Correig, B. Bouchikhi, E. Llobet, An electronic nose system based on a micro-machined gas sensor array to assess the freshness of sardines, Sensors and Actuators B: Chemical 141 (2009) 538–543.
93. G. Olafsdottir, E. Chanie, F. Westad, R. Jonsdottir, C.R. Thalmann, S. Bazzo, S. Labreche, P. Marcq, F. Lundby, J.E. Haugen, Prediction of microbial and sensory quality of cold smoked Atlantic salmon (Salmo salar) by electronic nose, JFS S: Sensory and Nutritive Qualities of Food 70 (2005) S563.
94. Ramin Yousefi, Muhamad Rasat Muhamad, Ali Khorsand Zak, Investigation of indium oxide as a self-catalyst in ZnO/ZnInO heterostructure nanowires growth, Thin Solid Films Volume 518, Issue 21, 31 August 2010, Pages 5971–5977.
95. M.A. Majeed Khan, Wasi Khan, Maqusood Ahamed, Mansour Alhoshan Structural and optical properties of In2O3 nanostructured thin film, Materials Letters Volume 79, 15 July 2012, Pages 119–121
96. Ramzan Muhammad, Structural, Electronic and Mechanical Properties of Advanced Functional Materials, PhD Thesis, URL: http://urn.kb.se/resolve?urn=urn:nbn:se:uu:diva-205243.
97. [97] M. Jothibas, C. Manoharan, S. Ramalingam, S. Dhanapandian, M. Bououdina, Spectroscopic analysis, structural, microstructural, optical and electrical properties of Zn-doped In2O3 thin films, Spectrochimica Acta Part A: Molecular and Biomolecular Spectroscopy Volume 122, 25 March 2014, Pages 171–178.
98. M. Jothibas, C. Manoharan, optical properties and Kubo gap analysis of In2O3 thin films, Appl. Surf. Sci. 98 (2003) 463-467.
99. N. M. A. Hadia, Santiago García-Granda, José R. García, Structural and optical properties of hydrothermally-synthesized single-crystalline In2O3 nanowires, Journal of the Korean Physical Society December 2013, Volume 63, Issue 11, pp 2143-2148.
100. H. Baqiah, N.B. Ibrahim, M.H. Abdi, S.A. Halim, Electrical transport, microstructure and optical properties of Cr-doped In2O3 thin film prepared by sol–gel method, Journal of Alloys and Compounds Volume 575, 25 October 2013, Pages 198–206.
101. Wen-Hui Zhang, Yi Sun, Li Park, synthesis and optical properties of nanosheet-based rh-In2O3 microflowers by triethylene glycol-mediated solvothermal process, J. Appl. Phys. 256 (2007) 124-127.
102. M. Öztas, M. Bedir, Z. Öztürk, D. Korkmaz and S. Sur, Structural and Optical Properties of Nanocrystal In2O3 Films by Thermal Oxidation of In2S3 Films, Chin. Phys. Lett. 23 1610 (2006).
103. A. A. Dakhel, Effect of ytterbium doping on the optical and electrical properties of intrinsic In2O3 thin films, Microelectronics Reliability Volume 50, Issue 2, February 2010, Pages 211–216.
104. Z. Galazka, G. Sbervilgiri, melt growth, characterization and properties of bulk In2O3 single crystal, Appl. Phys. Lett. 45 (2004) 154-158.
105. R.K. Gupta, K. Ghosh, S.R. Mishra, P.K. Kahol, High mobility W-doped In2O3 thin films: Effect of growth temperature and oxygen pressure on structural, electrical and optical properties, Applied Surface Science Volume 254, Issue 6, 15 January 2014, Pages 1661–1665.
106. S. Kaleemulla, N. Madhusudhana Rao, M. Girish Joshi, A. Sivasankar Reddy, S. Uthanna, P. Sreedhara Reddy, Electrical and optical properties of In2O3:Mo thin films prepared at various Mo-doping levels, Journal of Alloys and Compounds Volume 504, Issue 2, 20 August 2010, Pages 351–356.
107. Dali Shao, Liqiao Qin, Shayla Sawyer, Optical properties of polyvinyl alcohol (PVA) coated In2O3nanoparticles, Optical Materials Volume 35, Issue 3, January 2013, Pages 563–566.
108. A. Ayeshamariam, M. Bououdina, C. Sanjeeviraja, Optical, electrical and sensing properties of In2O3 nanoparticles, Materials Science in Semiconductor Processing Volume 16, Issue 3, June 2013, Pages 686–695.
109. Xiangying Chen, Zhongjie Zhang, Xingfa Zhang, Jianwei Liu, Yitai Qian, Single-source approach to the synthesis of In2S3 and In2O3crystallites and their optical properties, Chemical Physics Letters Volume 407, Issues 4–6, 27 May 2005, Pages 482–486.
110. Sergey K. Poznyak, Dmitri V. Talapin, and Anatoly I. Kulak , Structural, Optical, and Photoelectrochemical Properties of Nanocrystalline TiO2−In2O3 Composite Solids and Films Prepared by Sol−Gel Method, J. Phys. Chem. B, 2001, 105 (21), pp 4816–4823.
111. P. C. Lansaker, R. C. Febreauy, Chem. Phys. Lett. 58 (2013) 205-209.
112. G. Sahaya Bhaskaran, A. J. Luhia, J. G. Gupta, Structural role of In2O3 in PbO–P2O5–As2O3 glass system by means of spectroscopic and dielectric studies, Am. J. Phys. 14 (2007) 63-69.
113. J. Ederth, R. M. Kalsikar, Indium tin oxide films made from nanoparticles: models for the optical and electrical properties, Ceram. Int. 97 (2003) 11-17.
114. Dong Hoe Kim, Lee Sangwook, Jojhn Hoon Park, transmittance optimized Nb-doped TiO2/Sn-doped In2O3 multilayered photoelectrodes for dye-sensitized solar cells, Surf.
115. Jiali Zhai, Dejun Wang, Liang Peng, Yanhong Lin, Xinyong Li, Tengfeng Xie, Visible-light-induced photoelectric gas sensing to formaldehyde based on CdS nanoparticles/ZnO heterostructures, Sensors and Actuators B: Chemical, 147 (2010) 234-240.
116. Liang Peng, Pufeng Qin, Qingru Zeng, Huijuan Song, Ming Lei, Jubllant J.N. Mwangi, Dejun Wang, Tengfeng Xie, Improvement of formaldehyde sensitivity of ZnO nanorods by modifying with $Ru(dcbpy)_2(NCS)_2$, Sensors and Actuators B: Chemical, 160 (2011) 39-45.
117. Lexi Zhang, Jianghong Zhao, Jianfeng Zheng, Li Li, Zhenping Zhu, Shuttle-like ZnO nano/microrods: Facile synthesis, optical characterization and high formaldehyde sensing properties, Applied Surface Science, 258 (2011) 711-718.
118. Changsheng Xie, Liqi Xiao, Mulin Hu, Zikui Bai, Xianping Xia, Dawen Zeng, Fabrication and formaldehyde gas-sensing property of ZnO–MnO2 coplanar gas sensor arrays, Sensors and Actuators B: Chemical, 145 (2010) 457-463.
119. Lexi Zhang, Jianghong Zhao, Haiqiang Lu, Liming Gong, Li Li, Jianfeng Zheng, Hui Li, Zhenping Zhu, High sensitive and selective formaldehyde sensors based on nanoparticle-assembled ZnO micro-octahedrons synthesized by homogeneous precipitation method, Sensors and Actuators B: Chemical, 160 (2011) 364-370.
120. Yichuan Liao et al., Enhancement of photocatalytic property of ZnO for gaseous formaldehyde degradation by modifying morphology and crystal defect, Journal of Alloys and Compounds, 550 (2013) 190-197.

121. Zikui Bai, Changsheng Xie, Mulin Hu, Shunping Zhang, Formaldehyde sensor based on Ni-doped tetrapod-shaped ZnO nanopowder induced by external magnetic field, Physica E: Low-dimensional Systems and Nanostructures, 41 (2008) 235-239.
122. Xiangfeng Chu, Tongyun Chen, Wangbing Zhang, Banqiao Zheng, Hengfu Shui, Investigation on formaldehyde gas sensor with ZnO thick film prepared through microwave heating method, Sensors and Actuators B: Chemical, 142 (2009) 49-54.
123. Mohd Muzafa Jumidali, Kamal Mahir Sulieman, Md Roslan Hashim, Structural, optical and electrical properties of ZnO/Zn2GeO4 porous-like thin film and wires, Applied Surface Science, 257 (2011) 4890-4895.
124. JingWang, Peng Zhang, Jin-Qing Qi, Peng-Jun Yao, Silicon-based micro-gas sensors for detecting formaldehyde, Sensors and Actuators B 136 (2009) 399–404.
125. Weiwei Guo, Tianmo Liu∗, Rong Sun, Yong Chen, Wen Zeng, Zhongchang Wang, Hollow, porous, and yttrium functionalized ZnO nanospheres with enhanced gas-sensing performances, Sensors and Actuators B 178 (2013) 53– 62.
126. B. Cheng, E.T. Samulski, Hydrothermal synthesis of one-dimensional ZnO nanostructures with different aspect ratios, Chem. Commun. (2004) 986–987.
127. Z. Bai, C. Xie,M.Hu, S. Zhang, Formaldehyde sensor basedonNi-doped tetrapodshaped ZnO nanopowder induced by external magnetic field, Physica E 41 (2008) 235–239.
128. L. Peng, Q. Zhao, D. Wang, J. Zhai, P. Wang, S. Pang, T. Xie, Ultraviolet-assisted gas sensing: a potential formaldehyde detection approach at room temperature based on zinc oxide nanorods, Sens. Actuators B: Chem. 136 (2009) 80–85.
129. N.V. Hieu, N.D. Chien, Low-temperature growth and ethanol-sensing characteristics of quasi-one-dimensional ZnO nanostructures, Physica B 403 (2008) 50–56.
130. Y. Cao, P. Hu, W. Pan, Y. Huang, D. Jia, Methanal and xylene sensors based on ZnO nanoparticles and nanorods prepared by room-temperature solid-state chemical reaction, Sens. Actuators B: Chem. 134 (2008) 462–466.
131. K.N. Yu, Y. Xiong, Y. Liu, C. Xiong, Microstructural change of nano-SnO_2 grain assemblages with the annealing temperature, Phys. Rev. B 55 (1997) 2666–2671.
132. N. Yamazoe, G. Sakai, K. Shimanoe, Oxide semiconductor gas sensors, Catal. Surv. Asia 7 (2003) 63–75.
133. J. Xu, Q. Pan, Y. Shun, Z. Tian, Grain size control and gas sensing properties of ZnO gas sensor, Sens. Actuators B: Chem. 66 (2000) 277–279.
134. P.-S. Cho, K.-W. Kim, J.-H. Lee, Improvement of dynamic gas sensing behavior of SnO_2 acicular particles by microwave calcinations, Sens. Actuators B: Chem. 123 (2007) 1034–1039.
135. A. Srivastava, S.T. Lakshmikumar, A.K. Srivastava, R.J. Jain, Gas sensing properties of nanocrystalline SnO2 prepared in solvent media using a microwave assisted technique, Sens. Actuators B: Chem. 126 (2007) 583–587..
136. Nowack, B.; Bucheli, T. D. Environmental Pollution 2007, 150, 5-22.
137. Brayner, R.; Dahoumane, S. A.; Yèprelmian, C.; Djediat, C.; Meyer, M. l.; Coutel , A.; Fiel vet, F. Langmuir 2010, 26, 6522-6528.
138. Zhang, H.; Chen, B.; Banfield, J. F. The Journal of Physical Chemistry C 2010, 114, 14876-14884.
139. Liu, J.; Aruguete, D. M.; Murayama, M.; Hochella, M. F. Environmental Science & Technology 2009, 43, 8178-8183.
140. Zhang, Y.; Chen, Y.; Westerhoff, P.; Hristovski, K.; Crittenden, J. C. Water Research 2008, 42, 2204-2212.
141. Petosa, A. R.; Jaisi, D. P.; Quevedo, I. R.; Elimelech, M.; Tufenkji, N.Environmental Science & Technology 2010, 44, 6532-6549.
142. Tiede, K.; Hassellöv, M.; Breitbarth, E.; Chaudhry, Q.; Boxall, A. B. A. Journalof Chromatography A 2009, 1216, 503-509.
143. Grassian, V. H. The Journal of Physical Chemistry C 2008, 112, 18303-18313.
144. Abbas, Z.; Labbez, C.; Nordholm, S.; Ahlberg, E. The Journal of PhysicalChemistry C 2008, 112, 5715-5723.
145. Rao, C. N. R.; Kulkarni, G. U.; Thomas, P. J.; Edwards, P. P., Chemistry – A European Journal 2002, 8, 28-35.
146. Jolivet, J.-P.; Froidefond, C.; Pottier, A.; Chaneac, C.; Cassaignon, S.; Tronc, E.;Euzen, P. Journal of Materials Chemistry 2004, 14, 3281-3288.
147. Zhao, Q.; Xie, T.; Peng, L.; Lin, Y.; Wang, P.; Peng, L.; Wang, D. The Journal of Physical Chemistry C 2007, 111, 17136-17145.
148. Bian, S.-W.; Mudunkotuwa, I. A.; Rupasinghe, T.; Grassian, V. H. Langmuir2011, 27, 6059-6068.
149. G. Sberveglieri, G. Faglia, S. Groppelli, P. Nelli, A. Camanzi, A new technique for growing large surface-area SnO_2 thin-film (RGTO technique), Semiconductor Science And Technology 5 (1990) 1231–1233.
150. G. Faglia, E. Comini, A. Cristalli, G. Sberveglieri, L. Dori, Very low power consumption micromachined CO sensors, Sensors and Actuators B 55 (1999)140–146.
151. C. Garzella, E. Comini, E. Bontempi, L.E. Depero, C. Frigeri, G. Sberveglieri, Sol–gel TiO_2 and W/TiO_2 nanostructured thin films for control of drunkendriving, Sensors and Actuators B 83 (2002) 230–237.
152. E. Comini, G. Sberveglieri,V. Guidi, Ti–W–O sputtered thinfilmasnor p typegas sensors, Sensors and Actuators B 70 (2000) 108–114.
153. E. Comini, G. Faglia, G. Sberveglieri, CO and NO_2 response oftin oxide silicondoped thin films, Sensors and Actuators B 76 (2001) 270–274.
154. N. Yamazoe, New approaches for improving semiconductor gas sensors, Sensors and Actuators B 5 (1991) 7.
155. Joner, E. J. H., T.; Amundsen; C.E. Environmental fate and ecotoxicity of engineered nanoparticles, 2008.
156. French, R. A.; Jacobson, A. R.; Kim, B.; Isley, S. L.; Penn, R. L.; Baveye, P. C. Environmental Science & Technology 2009, 43, 1354-1359.
157. Cao, G. Nanostructures and nanomaterials; First ed.; Imperial college press: London, 2004.
158. Z. Miao, Y. Wu, X. Zhang, Z. Liu, B. Han, K. Ding, G. An, Large-scale production of self-assembled SnO_2 nanospheres and their application in high-performance chemiluminescence sensors for hydrogen sulfide gas, Journal of Materials Chemistry 17 (2007) 1791–1796.
159. S. Ho, A. Wong, G. Ho, Controllable porosity of monodispersed tin oxide nanospheres via an additive-free chemical route, Crystal Growth and Design 9 (2009) 732–736.
160. G. Korotcenkov, V. Brinzari, I. Boris, (Cu, Fe, Co or Ni)-doped tin dioxide films deposited by spray pyrolysis: doping influence on film morphology, Journal of Materials Science 43 (2008) 2761–2770.
161. X. Sun, X. Qiu, L. Li, G. Li, ZnO twin-cones: synthesis photoluminescence, and catalytic decomposition of ammonium perchlorate, Inorganic Chemistry 47 (2008) 4146–4152.
162. W. Li, E. Shi, W. Zhong, Z. Yin, Growth mechanism and growth habit of oxide crystals, Crystal Growth and Design 203 (1999) 186–196.
163. X. Wang, Q. Zhang, Q. Wan, G. Dai, C. Zhou, B. Zou, Controllable ZnO architectures by ethanolamine-assisted hydrothermal reaction for enhanced photocatalytic activity, The Journal of Physical Chemistry C 115 (2011) 2769–2775.
164. L. Xu, Y. Hu, C. Pelligra, C. Chen, L. Jin, H. Huang, S. Sithambaram, M. Aindow, R. Joesten, S. Suib, ZnO with different morphologies synthesized by solvothermal methods for enhanced photocatalytic activity, Chemistry of Materials 21 (2009) 2875–2885.
165. P. Hu, X. Zhang, N. Han, W. Xiang, Y. Cao, F. Yuan, Solution-controlled selfassembly of ZnO nanorods into hollow microspheres, Crystal Growth and Design 11 (2011) 1520–1526.
166. Kim P, Shi L, Majumdar A and McEuen P L 2001 Phys. Rev. Lett. 87 215502.
167. Schwab K, Henriksen E A, Worlock J M and Roukes M L 2000 Nature 404 974.
168. Shi L, Hao Q, Yu C, Kim D, Mingo N, Kong X Y and Wang Z L 2004 Appl. Phys. Lett. 84 2638.
169. Volz S G and Chen G 1999 Appl. Phys. Lett. 75 2056.
170. Sverdrup P G, Ju Y S and Goodson K E 2001 J. Heat Transfer 123 130.
171. Poncharal P, Wang Z L, Ugarte D and de Heer W A 1999 Science 283 1513.
172. Wang Z L, Poncharal P and de Heer W A 2000 Pure Appl. Chem. 72 209.
173. Gao R P, Wang Z L, Bai Z G, de Heer W A, Dai L M and Gao M 2000 Phys. Rev. Lett. 85 622.
174. Dai H J, Hafner J H, Rinzler A G, Colbert D T and Smalley R E 1996 Nature 384 147.
175. Hughes W and Wang Z L 2003 Appl. Phys. Lett. 82 2886.
176. Z. Fan, D. Wang, P. Chang, W. Tseng, J. Lu, ZnO nanowire field-effect transistorand oxygen sensing property, Appl. Phys. Lett. 85 (2004) 5923.
177. Z.L. Wang, Towards self-powered nanosystems: from nanogenerators to nanopiezotronics, Adv. Funct. Mater. 18 (2008) 3553–3567.
178. Y. Chin, R. Dagle, J. Hu, A. Dohnalkova, Y. Wang, Steam reforming of methanol over highly active Pd/ZnO catalyst, Catal. Today 77 (2002) 79–88.

Published By:
Blue Eyes Intelligence Engineering
& Sciences Publication (BEIESP)

179. Y. Choi, K. Futagami, T. Fujitani, J. Nakamura, The role of ZnO in Cu/ZnO methanol synthesis catalysts—morphology effect or active site model? Appl.Catal. A 208 (2001) 163–167.
180. T. Fujibayashi, T. Matsui, M. Kondo, Improvement in quantum efficiency of thin film Si solar cells due to the suppression of optical reflectance at transparent conducting oxide/Si interface by TiO2/ZnO antireflection coating, Appl. Phys. Lett. 88 (2006) 183508.
181. Z. Zhou, L. Chu, S. Hu, Microwave absorption behaviors of tetra-needle-like ZnO whiskers, Mater. Sci. Eng. B 126 (2006) 93–96.
182. Q.W. Li, J.I. Bian, J.C. Sun, J.W. Wang, Y.M. Luo, K.T. Sun, D.Q. Yu, Controllable growth of well-aligned ZnO nanorod arrays by low-temperature wet chemical bath deposition method, Applied Surface Science 256 (2010) 1698.
183. S. Xu, C.S. Lao, B.J. Weintraub, Z.L. Wang, Density-controlled growth of aligned ZnO nanowire arrays by seedless chemical approach on smooth surfaces, Journal of Materials Research 23 (2008) 2072.
184. J.Q. Xu, Y.P. Chen, D.Y. Chen, J.N. Shen, Hydrothermal synthesis and gas sensing characters of ZnO nanorods, Sensors and Actuators B 113 (2006) 526.
185. D. Barreca, E. Comini, A.P. Ferrucci, A. Gasparotto, C. Maccato, C. Maragno, G. Sberveglieri, E. Tondello, First example of ZnO-TiO2 nanocomposites by chemical vapor deposition: structure, morphology, composition, and gas sensing performances, Chemistry of Materials 19 (2007) 5642.
186. C.X. Wang, L.W. Yin, L.Y. Zhang, Y.X. Qi, N. Lun, N.N. Liu, Large scale synthesis and gas-sensing properties of anatase TiO2 three-dimensional hierarchical nanostructures, Langmuir 26 (2010) 12841.
187. N.V. Quy, V.A. Minh, N.V. Luan, V.N. Hung, N.V. Hieu, Gas sensing properties at room temperature of a quartz crystal microbalance coated with ZnO nanorods, Sensors and Actuators B 153 (2011) 188.
188. G.W. Sauerbrey, The use of quartz crystal oscillators for weighting thin layer and for microweighing, Zeitschrift für Physik 155 (1959) 206.
189. G.W. Sauerbrey, The use of quartz crystal oscillators for weighting thin layer and for microweighing, Zeitschrift für Physik 155 (1959) 206.
190. K. Kleo, A. Kapp, L. Ascher, F. Lisdat, Detection of vaccinia virus DNA by quartz crystal microbalance, Analytical Biochemistry 418 (2011) 260.
191. T. Seiyama, A. Kato, K. Fujiishi, M. Nagatani, A new detector for gaseous components using semiconductive thin films, Anal. Chem. 34 (1962) 1502–1503.
192. W.-T. Yao, S.-H. Yu, Recent advances in hydrothermal syntheses of low dimensional nano architectures, Int. J. Nanotechnol. 4 (2007) 129–162.
193. K. Byrappa, T. Adschiri, Hydrothermal technology for nanotechnology, Progr. Cryst. Growth Charact. Mater. 53 (2007) 117–166.
194. S. Jain, D.J. Skamser, T.T. Kodas, Morphology of single-component particles produced by spray pyrolysis, Aerosol Sci. Technol. 27 (1997) 575–590.
195. S.H. Ju, Y.C. Kang, Fine-sized LiBi0.8Co0.15Mn0.05O2 cathode powders prepared by combined process of gas-phase reaction and solid-state reaction methods, J. Power Sources 178 (2008) 387–392.
196. L. Zhang, J. Zhao, J. Zheng, L. Li, Z. Zhu, Hydrothermal synthesis of hierarchical nanoparticle-decorated ZnO microdisks and the structure-enhanced acetylene sensing properties at high temperatures, Sens. Actuators B 158 (2011) 144–150.
197. T.J. Hsueh, Y.W. Chen, S.J. Chang, S.F. Wang, C.L. Hsu, Y.R. Lin, T.S. Lin, I.C.
198. Chen, ZnO nanowire-based CO sensors prepared at various temperatures, J. Electrochem. Soc. 154 (2007) J393–J396.
199. P. Feng, Q. Wan, T.H. Wang, Contact-controlled sensing properties of flowerlike ZnO nanostructures, Appl. Phys. Lett. 87 (2005) 213111.
200. Y.J. Chen, C.L. Zhu, G. Xiao, Reduced-temperature ethanol sensing characteristics of flower-like ZnO nanorods synthesized by a sonochemical method, Nanotechnology 17 (2006) 4537–4541.
201. Y. Zhang, J.Q. Xu, Q. Xiang, H. Li, Q.Y. Pan, P.C. Xu, Brush-like hierarchical ZnO nanostructures: synthesis, photoluminescence and gas sensor properties, J. Phys. Chem. C 113 (2009) 3430–3435.
202. M. Ohyama, H. Kozuka, T. Yoko, Sol–gel preparation ofZnOfilmswith extremely preferred orientation along (0 0 2) plane from zinc acetate solution, Thin Solid Films 306 (1997) 78–85.
203. L. Vayssieres, K. Keis, A. Hagfeldt, S.E. Lindquist, Three-dimensional array of highly oriented crystalline ZnO microtubes, Chem. Mater. 13 (2001) 4395–4398.
204. X.F. Wu, H. Bai, C. Li, G. Lu, G.Q. Shi, Controlled one-step fabrication of highly oriented ZnO nanoneedle/nanorods arrays at near room temperature, Chem. Commun. 15 (2006) 1655–1657.
205. M. Gratzel, Photoelectrochemical cells, Science 414 (2001) 338–344.
206. Q.H. Li, Y.X. Liang, Q. Wan, T.H. Wang, Oxygen sensing characteristics of individual ZnO nanowire transistors, Appl. Phys. Lett. 85 (2004) 6389–6391.
207. J.X. Wang, X.W. Sun, S.S. Xie, Y. Yang, H.Y. Chen, G.Q. Lo, D.L. Kwong, Preferential growth of SnO2 triangular nanoparticles on ZnO nanobelts, J. Phys. Chem. C 111 (2007) 7671–7675.
208. F. Xu, Y.N. Lu, Y. Xie, Y.F. Liu, Synthesis and photoluminescence of assemblycontrolled ZnO architectures by aqueous chemical growth, J. Phys. Chem. C 113 (2009) 1052–1059.
209. K. Vanheusden, C.H. Seager, W.L. Warren, D.R. Tallant, J.A. Voigt, Correlation between photoluminescence and oxygen vacancies in ZnO phosphors, Appl. Phys. Lett. 68 (1996) 403–405.
210. A. Anastasiou, M.H.J. Lee, C. Leach, R. Freer, Ceramic varistors based on ZnO–SnO2, Journal of the European Ceramic Society 24 (2004) 1171.
211. H.Y. Yang, S.F. Yu, H.K. Liang, R.G. Mote, C.W. Cheng, H.J. Fan, T. Sun, H.H. Hng, High-temperature lasing characteristics of randomly assembled SnO_2 backbone nanowires coated with ZnO nanofins, Journal of Applied Physics 106 (2009) 123105–123115.
212. [12] W. Chen, Y. Qiu, Y. Zhong, K.S. Wong, S.H. Yang, High-efficiency dye-sensitized solar cells based on the composite photoanodes of SnO2 nanoparticles/ZnO nanotetrapods, Journal of Physical Chemistry A 114 (2010) 3127–3138.
213. C. Liangyuan, B. Shouli, Z. Guojun, L. Dianqing, C. Aifan, C.C. Liu, Synthesis of ZnO–SnO2 nanocomposites by microemulsion and sensing properties for NO_2, Sensors and Actuators B: Chemical 134 (2008) 360–366.
214. W.-H. Zhang, W.-D Zhang, Fabrication of SnO_2–ZnO nanocomposite sensor for selective sensing of trimethylamine and the freshness of fishes, Sensors and Actuators B: Chemical 134 (2008) 403–408.
215. X. Song, L. Liu, Characterization of electrospun ZnO–SnO2 nanofibers for ethanol sensor, Sensors and Actuators A: Physical 154 (2009) 175–179.
216. J.Y. Park, S.S. Kim, Growth of nanograins in electrospun ZnO nanofibers, Journal of the American Ceramic Society 92 (2009) 1691–1694.
217. C.V. Manzano, D. Alegre, O. Caballero-Calero, B. Alén, M.S. Martín-González, Synthesis and luminescence properties of electrodeposited ZnO films, Journal of Applied Physics 110 (2011) 043538.
218. M.W. Ahn, K.S. Park, J.H. Heo, D.W. Kim, K.J. Choi, J.G. Park, On-chip fabrication of ZnO-nanowire gas sensor with high gas sensitivity, Sensors and Actuators B 138 (2009) 168.
219. J. Singh, S.S. Patil, M.A. More, D.S. Joag, R.S. Tiwari, O.N. Srivastava, Formation of aligned ZnO nanorods on self-grown ZnO template and its enhanced field emission characteristics, Applied Surface Science 256 (2010) 6157.
220. Y. Ye, R. Lim, J.M. White, High mobility amorphous zinc oxynitride semiconductor material for thin film transistors, Journal of Applied Physics 106 (2009) 074512.
221. A. Umar, M.M. Rahman, A. Al-Hajry, Y.B. Hahn, Highly-sensitive cholesterol biosensor based on well-crystallized flower-shaped ZnO nanostructures, Talanta 78 (2009) 284.
222. T.L. Phan, S.C. Yu, R. Vincent, N.H. Dan, W.S. Shi, Photoluminescence properties of various CVD-grown ZnO nanostructures, Journal of Luminescence 130 (2010) 1142.
223. L.B. Feng, A.H. Liu, M. Liu, Y. Ma, J. Wei, B.Y. Man, Fabrication and characterization of tetrapod-like ZnO nanostructures prepared by catalyst-free thermal evaporation, Materials Characterization 61 (2010) 128.
224. I.C. Robin, P. Marotel, A.H. El-Shaer, V. Petukhov, A. Bakin, A. Waag, M. Lafossas, J. Garcia, M. Rosina, A. Ribeaud, S. Brochen, P. Ferret, G. Feuillet, Compared optical properties of ZnO heteroepitaxial, homoepitaxial 2D layers and nanowires, Journal of Crystal Growth 311 (2009) 2172.
225. R.J. Mendelsberg, M. Kerler, S.M. Durbin, R.J. Reeves, Photoluminescence behavior of ZnO nanorods produced by eclipse PLD from a Zn metal target, Superlattices and Microstructures 43 (2008) 594.
226. B.A. Taleatu, A.Y. Fasasi, G. Di Santo, S. Bernstorff, A. Goldoni, M. Fanetti, L. Floreano, P. Borghetti, L. Casalis, B. Sanavio, C. Castellarin-Cudia, Electro-chemical deposition of zinc oxide nanostructures by using two electrodes, AIP Advances 1 (2011) 032147.

227. M.J. Height, L. Mädler, S.E. Pratsinis, Nanorods of ZnO made by flame spray pyrolysis, Chemistry of Materials 18 (2006) 572.
228. Q. Li, V. Kumar, Y. Li, H. Zhang, T.J. Marks, H.P.R. Chang, Fabrication of ZnO nanorods and nanotubes in aqueous solutions, Chemistry of Materials 17 (2005) 1001.
229. P.A. Lieberzeit, A. Rehman, B. Najafi, F.L. Dickert, Real-life application of a QCM based e-nose: quantitative characterization of different plant-degradation processes, Analytical and Bioanalytical Chemistry 391 (2008) 2897.
230. Xianfeng Wang, Fuhai Cui, Jinyou Lin, Bin Ding, Jianyong Yu,∗∗, Salem S. Al-Deyab, Functionalized nanoporous TiO_2 fibers on quartz crystal microbalance platform for formaldehyde sensor, Sensors and Actuators B 171– 172 (2012) 658– 665.
231. H.H. Lou, Y. Zhang, Q. Xiang, J.Q. Xu, H. Li, P.C. Xu, X.X. Li, The real-time detection of trace-level Hg2+ in water by QCM loaded with thiol-functionalized SBA-15, Sensors and Actuators B 166–167 (2012) 246.
232. J. Ito, T. Nakamoto, H. Uematsu, Discrimination of halitosis substance using QCM sensor array and a preconcentrator, Sensors and Actuators B 99 (2004) 431.
233. M.M. Ayad, N.L. Torad, Alcohol vapours sensor based on thin polyaniline salt film and quartz crystal microbalance, Talanta 78 (2009) 1280.
234. P. Sun, Y.D. Jiang, G.Z. Xie, X.S. Du, J. Hu, A room temperature supramolecularbased quartz crystal microbalance (QCM) methane gas sensor, Sensors and Actuators B 141 (2009) 104.
235. M.N.R. Ashfold, R.P. Doherty, N.G. Ndifor-Angwafor, D.J. Riley, Y. Sun, The kinetics of the hydrothermal growth of ZnO nanostructures, Thin Solid Films 515 (2007) 8679.

AUTHORS PROFILE

Assistant teacher **:** naser hussein judran sumer university /fasulty of basic education (physics ministy of education www: uso. edu.iqeducation:master of physics scince /nano materaluniversity:sam higgin bottom institute ,deprtment: physics graduation:2012-2014 skills:nanou application,

Mr. Ajeet Kumar, He is MSc. in Physics from the Department of Physics, SHIATS, Allahabad. He has completed his BSc. from Kanpur University. His research interest includes superconductivity and nano-materials.